Front. Mech. Eng. 2023, 18(2): 21
https://doi.org/10.1007/s11465-022-0737-8

RESEARCH ARTICLE

Build orientation determination of multi-feature mechanical parts in selective laser melting via multi-objective decision making

Hongsheng SHENG[c], Jinghua XU[a,b,c], Shuyou ZHANG (✉)[a,b,c], Jianrong TAN[a,b,c], Kang WANG[c]

[a] *State Key Laboratory of Fluid Power and Mechatronic Systems, Hangzhou 310027, China*
[b] *Key Laboratory of Advanced Manufacturing Technology of Zhejiang Province, Hangzhou 310027, China*
[c] *Engineering Research Center for Design Engineering and Digital Twin of Zhejiang Province, Zhejiang University, Hangzhou 310027, China*

✉ *Corresponding author. E-mail: zsy@zju.edu.cn (Shuyou ZHANG)*

ABSTRACT Selective laser melting (SLM) is a unique additive manufacturing (AM) category that can be used to manufacture mechanical parts. It has been widely used in aerospace and automotive using metal or alloy powder. The build orientation is crucial in AM because it affects the as-built part, including its part accuracy, surface roughness, support structure, and build time and cost. A mechanical part is usually composed of multiple surface features. The surface features carry the production and design knowledge, which can be utilized in SLM fabrication. This study proposes a method to determine the build orientation of multi-feature mechanical parts (MFMPs) in SLM. First, the surface features of an MFMP are recognized and grouped for formulating the particular optimization objectives. Second, the estimation models of involved optimization objectives are established, and a set of alternative build orientations (ABOs) is further obtained by many-objective optimization. Lastly, a multi-objective decision making method integrated by the technique for order of preference by similarity to the ideal solution and cosine similarity measure is presented to select an optimal build orientation from those ABOs. The weights of the feature groups and considered objectives are achieved by a fuzzy analytical hierarchy process. Two case studies are reported to validate the proposed method with numerical results, and the effectiveness comparison is presented. Physical manufacturing is conducted to prove the performance of the proposed method. The measured average sampling surface roughness of the most crucial feature of the bracket in the original orientation and the orientations obtained by the weighted sum model and the proposed method are 15.82, 10.84, and 10.62 μm, respectively. The numerical and physical validation results demonstrate that the proposed method is desirable to determine the build orientations of MFMPs with competitive results in SLM.

KEYWORDS selective laser melting (SLM), build orientation determination, multi-feature mechanical part (MFMP), fuzzy analytical hierarchy process, multi-objective decision making (MODM)

1 Introduction

Additive manufacturing (AM) is an advanced freeform fabrication process that fabricates a physical part from its three-dimensional digital model using layer-upon-layer material deposition [1]. This unique manufacturing mechanism gives AM several advantages regarding material saving, design flexibility, high feasibility for geometric complexity, and shorter development time for new products compared with conventional subtractive manufacturing processes [2,3]. AM processes are divided into seven categories [4], in which selective laser melting (SLM) [1], also known as laser powder bed fusion or direct metal laser melting, helps directly manufacture complex shape parts with high mechanical performance and accuracy from metal or alloy powder particles without the mold design process [3]. This characteristic of the SLM process makes it desirable for fabricating high-quality mechanical parts widely used in aerospace and automotive.

The SLM process consists of powder material deposition on a platform or previous as-built layer, selective fusion of powder particles by a laser beam based on the current layer's profile, lowering the platform by a

Received April 17, 2022; accepted August 22, 2022

predefined layer thickness, and recoating a new layer of powder material. The cycle repeats until the entire part is fabricated. This process will generate a staircase effect on the surface of an SLM part [2]. The staircase effect adversely affects the surface quality of an SLM part and cannot be eliminated. The mechanical part usually has multiple surface features, such as cylindrical and planar features, which are used for connection, mating, bearing, and assembly. For a multi-feature mechanical part (MFMP), the poor surface quality, especially on the working surface, will influence its usage function. In practice, a surface finishing process is essential to improve the surface quality of an as-built part in AM [5–7]. However, it requires additional time and cost. To improve this shortcoming, feasible process planning is crucial for the SLM process.

Process planning for an SLM part mainly includes the build orientation determination, support structure generation, slice creation, laser scanning path planning, and process parameters determination [8,9]. The build orientation is essential because it directly affects the subsequent support structure generation, slice creation, and laser scanning path planning [10,11]. The build orientation of an SLM part has a critical effect on the mechanical properties, part accuracy, surface quality, support volume, and build time and cost of its as-built part [12–17]. The build orientation determination for an SLM part involves selecting an optimal build orientation (OBO) from the infinite build orientation space regarding the part's particular production or design requirements. A desirable OBO is critical to the fabrication of an MFMP in SLM. It is difficult to manually select a suitable OBO to benefit the as-built part in practice comprehensively.

Many studies have been performed to determine an OBO for different AM processes, such as fused deposition modeling (FDM) [18–29], stereolithography (SLA) [20–23,30–35], selective laser sintering (SLS) [20–22,36–39], and SLM [12–15,40]. Methods in previous studies can be classified into computation-based and evaluation methods [25,33,39]. The computation-based methods adopt optimization methods to directly obtain one or more OBOs regarding single or multiple optimization objectives by global searching from the infinite orientation space [12–15,18–21,25–29,34–37]. The evaluation methods select an OBO from a set of alternative build orientations (ABOs) using multi-objective decision making (MODM) by considering the objectives affected by build orientation [22–24,30–33,38–42]. The objective estimation accuracy is crucial to the ultimate achieved OBO. However, several objective estimation methods in the literature are either unsuitable for SLM [19,23,36,37] or not sufficiently accurate (e.g., the support volume, and build time and cost [12,42]).

This study attempts to determine the OBOs for MFMPs in SLM. For an MFMP, its surface features are critical in conventional machining and AM processes. It carries the information on the design or functional requirements of the part [39]. The specific knowledge of the features can be utilized in determining the OBO. A method to determine the OBOs for MFMPs in SLM via MODM is developed in this study. The method initially identifies the surface features of an MFMP and groups them to formulate specific optimization objectives. The estimation accuracy of the support volume, and build time and cost are improved to increase the trustworthiness of the computation results. Then, the ABOs are generated by many-objective optimization (MOO). Ultimately, an integrated MODM method is presented to select an OBO from the ABOs.

This study is organized as follows. Section 2 reviews the related work. Section 3 introduces the framework of the proposed method. Section 4 validates the effectiveness of the proposed method with two MFMPs, and offers physical experiments and a discussion. Section 5 ends this study with conclusions.

2 Related work

2.1 Computation-based methods for OBO determination

Computation-based methods are intuitive ways to obtain one or more OBOs for an AM part by applying an exhaustive search method to traverse the infinite orientation space. Many types of exhaustive search method have been conducted in the literature, such as nonlinear optimization-based methods [12,29,37,43,44], population-based optimization algorithms [13,14,18–21,26,27,34–36,45], Taguchi method [25], derivative-free simulated annealing method [28], and Tabu search method [15]. Morgan et al. [12] determined the OBO for an SLM part by minimizing the support volume using a line search algorithm. They calculated the support volume by summing the volume of the irregular prism formed by each downward facet and the build platform. Nonetheless, this estimation method is inaccurate for the commonly applied nonconvex model because, in this case, certain prisms will intersect the model instead of the platform [22]. Similar estimation methods were also implemented in Refs. [23,25,33,34].

Wang and Qian [29] proposed a method to simultaneously optimize the build orientation and topology layout of an FDM part by moving asymptotes. Singhal et al. [37] considered the surface roughness, build time, and the quantity of support structure in the OBO determination for SLA and SLS processes by the trust region method. Their approach utilized the part height along the *z*-direction to estimate the build time, which was a simple and efficient computation method. Although they considered the influence of support structure on estimating build time, the entire area of the supported facets was taken as the quantity of support structure. This estimation was not desirable because the actual support volume was also affected by the height of the supported facets. This shortcoming likewise appeared in Refs. [19,26,27].

Paul and Anand [43] utilized the weighted sum model (WSM) to convert the multiple optimization objectives into a single main objective. In this manner, the build orientation could be optimized using the trust region method, which would minimize the part's flatness, cylindricity errors, and support volume. They reported a voxel-based method to calculate the support volume. The method required converting the input standard tessellation language (STL) model into a voxel representation, which induced a high computation cost, especially for computation-based methods with many iterations [24]. This method was also applied in Refs. [14,44]. Chowdhury et al. [44] determined the OBO by the WSM based on a global search algorithm in MATLAB software. The geometric features, support volume, support contact area, mean cusp height, and build time were involved. They measured the build time only by the number of layers, resulting in an inaccurate result. Nonlinear optimization-based methods have an issue with the definition of search step size that influences the balance between effectiveness and efficiency [17].

Population-based optimization algorithms are the most popular computation-based methods, such as genetic algorithm (GA) [13,18,20,21,34,36], particle swarm optimization [14], and non-dominated sorting genetic algorithm II (NSGA-II) [19,27,35]. In comparison with nonlinear optimization-based methods, population-based optimization algorithms are conducive for improving solving efficiency. Masood et al. [18] determined the best part orientation by minimizing the volumetric error using GA. They calculated the volumetric error by the layer thickness and the area difference between each layer's top and bottom slices. Pandey et al. [19] simultaneously optimized the surface roughness and build time by the NSGA-II to obtain the Pareto front. The OBO could be obtained from the Pareto front based on minimum build time or surface roughness.

Byun and Lee [20] proposed a method to determine the OBO in FDM and SLA processes by the WSM, considering the surface roughness and build time. However, their approach did not provide the estimation method of the support volume, and the corresponding estimated build time is inaccurate. Ahn et al. [21] optimized the build orientation by minimizing the surface roughness using GA. Canellidis et al. [34] implemented the WSM to achieve an OBO in SLA regarding the build time and surface roughness. The support removal time was considered in estimating build time. Phatak and Pande [36] utilized the WSM to determine an OBO for an SLS part, considering the part build height, surface roughness, and material utilization.

Brika et al. [13] determined the OBO of an SLM part by the WSM, and the considered objectives included the mechanical properties, surface roughness, support volume, and build time and cost. Cheng and To [14] utilized the WSM to obtain the OBO of an SLM part with minimum residual stress and support volume. Griffiths et al. [15] proposed a build cost estimation method for an SLM part and applied it to address the problem of obtaining an OBO and 2D irregular bin packing a mixed batch of parts across identical SLM machines. Matos et al. [26] selected the volumetric error, support area, staircase effect, build time, surface roughness, and surface quality as the optimization objectives to obtain an OBO for an FDM part using an electromagnetism-like mechanism algorithm. They further adopted a MOO method to optimize the volumetric error, support area, build time, and surface roughness simultaneously to achieve the OBO by NSGA-II [27]. Nevertheless, they used the support area and part height to estimate the amount of support and build time, respectively, which, as previously mentioned, was inaccurate.

Ulu et al. [28] introduced a model shape correction method in AM and optimized the build orientation by minimizing the difference between the modified shape and the manufactured part. Mele and Campana [35] applied the evolutionary algorithms to obtain the OBO that was the one with the lowest cost, evaluated by the material mass and build time. The input mesh was initially simplified in their method to reduce the computation cost. However, this method would damage the accuracy of the computation results. In addition to the methods above, several studies have applied machine learning techniques to optimize the build orientation to reduce user-preferred features' support or improve prediction accuracy on the build time and part mass [46,47].

The WSM is a convenient and efficient means to determine a build orientation with multiple objectives. Unfortunately, the WSM does not work well in the case of MOO with nonconvex Pareto fronts [48], which frequently appears in build orientation issues with multiple objectives.

Although the applications of computation-based methods require more calculation costs, they will achieve more accurate results. Computation-based methods are widely applied for the build orientation determination of an AM part.

2.2 Evaluation methods for OBO determination

Evaluation methods determine the OBO of an AM part by generating a set of ABOs and then selecting the most optimal via specific methods. The typical generation methods of ABOs can be classified into feature-based methods [30–32,39,40], convex hull generation method [22], facet clustering methods [41,42], and quaternion rotation methods [23,33]. Cheng et al. [30] developed a classification method of the features of 3D models and applied such features to generate the ABOs. For example, the normal vector of a planar feature was selected as an ABO. The OBO was determined by the part accuracy and build time one by one, which did not consider the trade-off between the objectives. Pham et al. [31] reported similar work, but they were concerned with the support volume, and build time and cost. West et al. [32] proposed a process planning system to select the desirable build orientation, layer thickness, and recoating variables for an SLA part. The ABOs were identified by the typical surface features of the part, and the OBO was determined by a deviation function regarding the surface roughness, part accuracy, and build time.

Zhang et al. [39] indicated the definition of AM features and classified the AM features into cylindrical, planar, tapered, and structural unit types combined by the former three. The ABOs were generated from the recognized AM features via specific rules, such as two orientations perpendicular to a planar feature as its ABOs. The OBO was selected based on an MODM method regarding the surface roughness, support volume, build time and cost, and favorableness of AM features. The estimated objective values depended on a process planning platform named KARMA Tool. Al-Ahmari et al. [40] performed a method to read a model of the Standard for the Exchange of Product Model Data to extract its features and geometric properties. They applied the recognized features to generate the ABOs. The generation rules were similar to the feature-based methods above. The OBO was determined based on the WSM, considering the accuracy and build time. Feature-based methods are not suitable for the freeform surface models because the feature definition of such models is difficult.

Byun and Lee [22] manually selected the normal vectors of the surfaces of the convex hull of the STL model as the ABOs. The surface roughness and build time and cost were considered the evaluation objectives to obtain the OBO using the WSM. The accuracy issue limits the convex hull generation method because the convex hull is not the exact model. Zhang et al. [41] divided the STL model into several finite clusters of significant triangular facets based on the similarity of the facet normal vectors based on the *k*-means clustering algorithm. The unitized central vector of all normal vectors in a cluster and its opposite vector served as this cluster's ABOs. The facet clustering method is efficient because it avoids the AM feature recognition and can also be applied for freeform surface models. Qin et al. [42] improved the computation efficiency and stability of the generation of ABOs in Ref. [41] using an accelerated hierarchical density-based spatial clustering of applications with noise* algorithm instead of the *k*-means clustering algorithm. The WSM determined the OBO for an SLM part regarding the support volume, surface roughness, volumetric error, build time, and build cost. The support volume was estimated by Autodesk Meshmixer software, which had computation efficiency and convenience limitations because the software required frequent operations for the ABOs. The ABO generation rule of the facet clustering methods is similar to feature-based and convex hull generation methods.

The above three evaluation methods require little computation time because they focus on a few ABOs in the finite possible build orientations [17]. The quality of the obtained OBO is highly dependent on the ABOs. Selecting the normal vector of a feature or a facet cluster as the ABO is advantageous to the surface quality of the planar surface but may be disadvantageous to that of the nonplanar surface, such as cylindrical surface. In addition, the calculation of the actual support volume of an AM part is complex [24]. This ABO generation rule cannot guarantee to benefit from the reduction of the support volume.

Qie et al. [33] determined ABOs by rotating a model around a randomly acquired axis using quaternion rotation, which made the search space of the ABOs expand to infinity. A feedback MODM model iteratively achieved the OBO until the user's requirements were satisfied, in which the surface roughness, support volume, and build time were concerned. Yu et al. [23] improved the work of Ref. [33] by proposing a negative feedback decision-making model, and the build cost and flatness error were added to the optimization objectives. Given that the rotation axis was created randomly, the quaternion rotation methods could miss the true OBO in the obtained ABOs.

In addition to the four evaluation methods above, Padhye and Deb [38] applied the NSGA-II and multi-objective particle swarm optimization to obtain the ABOs in the Pareto front of an SLS part, considering the surface roughness and build time. They proposed three decision-making methods to select the best one from the Pareto ABOs. Di Angelo et al. [24] developed a similar approach to obtain the Pareto ABOs for an FDM part, considering the surface quality and build cost by the *S*-metric selection evolutionary multi-objective algorithm. The OBO was determined by the technique for order of preference by similarity to ideal solution (TOPSIS) [49].

The present study is motivated by the two types of OBO determination method and thus proposes an approach to determine an OBO for an MFMP in SLM with desirable results.

3 Framework of the proposed method

The schematic of the proposed method is presented in Fig. 1. The input includes the manifold mesh model and machining accuracy design requirements (MADRs) of an

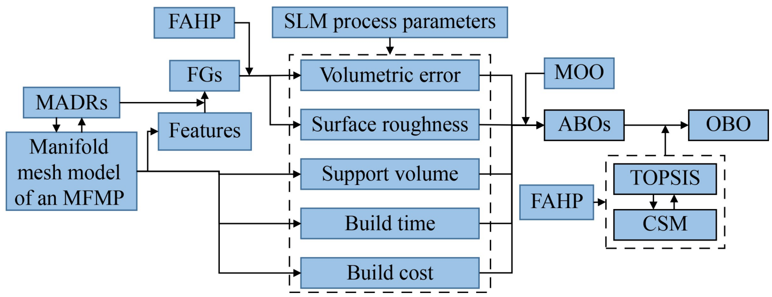

Fig. 1 Schematic of the proposed method. ABO: alternative build orientation, CSM: cosine similarity measure, FAHP: fuzzy analytical hierarchy process, FG: feature group, MADR: machining accuracy design requirement, MFMP: multi-feature mechanical part, MOO: many-objective optimization, OBO: optimal build orientation, SLM: selective laser melting, TOPSIS: technique for order of preference by similarity to ideal solution.

MFMP and SLM process parameters, such as layer thickness, recoating time, laser scanning velocity, and hatch spacing. The main steps of the proposed method consist of feature recognition and grouping, generation of ABOs, and OBO determination.

In feature recognition and grouping, the features of the input model are recognized, and the features with the same MADR are combined into a feature group (FG). In the generation of ABOs, the estimation models of the optional optimization objectives, namely volumetric error, surface roughness, support volume, and build time and cost, are established. The values of volumetric error and surface roughness are the weighted sums of the values of the FGs, following their MADRs. Then, the ABOs are generated by the MOO regarding the considered objectives. In OBO determination, an OBO is selected from the ABOs based on an integrated MODM method composed of the TOPSIS and cosine similarity measure (CSM) [50]. The weights of the FGs and considered objectives are defined by the fuzzy analytical hierarchy process (FAHP) [51]. Finally, the OBO and its objective estimation values are the outputs. The details of the proposed method are described in the following sections.

3.1 Feature recognition and grouping

Whether in conventional or AM process planning, the MADR (can be expressed by surface roughness) of a specific feature of an MFMP should be given more attention because it affects the part's function realization and machining cost. To this end, the surface features of an MFMP should be initially recognized, especially in the AM environment. Moroni et al. [52] identified the cylindrical assembly feature from the STL model to serve as the build orientation consideration for the surface quality of a functional assembly component fabricated by AM. Zhang et al. [39] classified the AM features into cylindrical, planar, tapered, and structural unit types combined by the former three types. These features are the typical features of mechanical parts. The other standard features of mechanical parts include the spherical and rotational features and can likewise be utilized in AM. Given that the input model is a manifold mesh model, the dihedral angle method is applied to obtain the surface features of an MFMP [53].

Different features of an MFMP will have different MADRs in accordance with their various functions. Consequently, the build orientation should benefit the features with high MADRs. Generally, an MFMP has several MADRs; its features with the same MADR will have different positions and directions. It is not easy to select a build orientation to optimize all of them simultaneously. To this end, those features can be regarded as a whole, that is, the features with the same MADR form an FG.

Figure 2 illustrates the above process. Figure 2(a) depicts the 20 recognized features of an MFMP, including cylindrical and planar features. The central cylindrical feature has the highest MADR. The planar mating features (including the bottom planar feature) intersecting with the middle cylindrical features have the same MADR and are smaller than the central cylindrical feature. The two small cylindrical features used as the connecting bolts have the same MADR and are smaller than the former two MADRs. The remaining features have the same and lowest MADR. The four MADRs and the combined FGs are shown in Fig. 2(b), where the features with the same color represent an FG.

3.2 Generation of ABOs

The objective estimation models should be reasonable and practical to obtain more accurate optimization results. Indeed, a desirable MOO solving method is crucial for the generation of ABOs. The details are presented in this section.

3.2.1 Objective estimation models

In this study, the volumetric error, surface roughness, support volume, and build time and cost are considered as the optimization objectives for determining the build orientation of an MFMP in SLM.

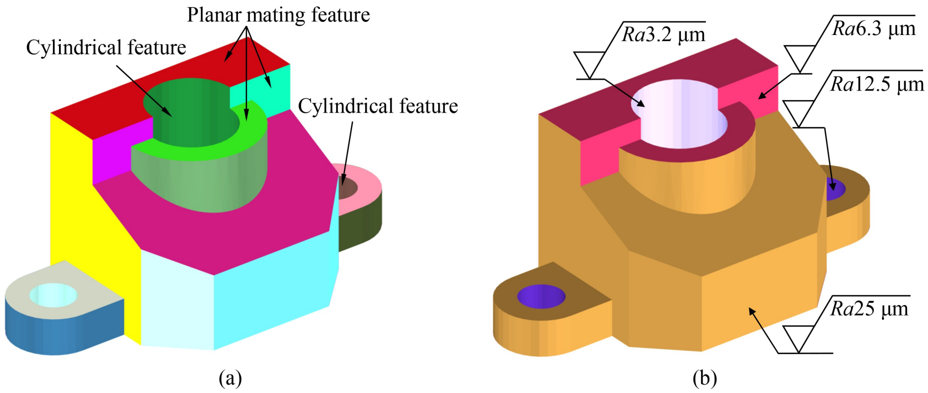

Fig. 2 Illustration of the (a) features and (b) feature groups of a multi-feature mechanical part.

(1) Volumetric error model. The existence of the staircase effect results in a volumetric difference or volumetric error as shown in Fig. 3. The volumetric error is the difference between the volume of the material used for the AM part and the volume specified by the manifold model [18,42,45,54]. The volumetric error affects the part shape accuracy of an as-built part in AM and cannot be eliminated [45]. The model for estimating the entire volumetric error, VE, of an AM part is expressed as follows [42,45]:

$$VE = \sum_{i=1}^{n_{\mathrm{f}}} \frac{l_{\mathrm{t}} \left| \boldsymbol{d} \cdot \boldsymbol{n}_i^{\mathrm{f}} \right|}{2} A_i^{\mathrm{f}}, \tag{1}$$

where l_{t} is the layer thickness, $\boldsymbol{d} = (0, 0, 1)^{\mathrm{T}}$ is the build direction vector, A_i^{f} and $\boldsymbol{n}_i^{\mathrm{f}}$ are the area and unit normal vector of the ith facet F_i, respectively, and n_{f} is the number of facets of the manifold model. In Fig. 3, α_i is the angle between the build direction $\boldsymbol{d}$ and normal vector of the ith facet $\boldsymbol{n}_i^{\mathrm{f}}$. The build orientation and layer thickness directly influence the volumetric error.

Given that the FGs have different MADRs, Eq. (1) cannot reflect the relative importance of different FGs. A weight is assigned to the volumetric error produced by each FG, and the weighted volumetric error, V_{wve}, of an SLM part can be obtained by

$$V_{\mathrm{wve}} = \sum_{i=1}^{n_{\mathrm{fg}}} w_i^{\mathrm{fg}} VE_i^{\mathrm{fg}}, \tag{2}$$

where n_{fg} is the number of the FGs, w_i^{fg} ($w_i^{\mathrm{fg}} > 0$) and VE_i^{fg} are the weight and volumetric error of the ith FG, respectively, and $\sum_{i=1}^{n_{\mathrm{fg}}} w_i^{\mathrm{fg}} = 1$.

A higher weighted volumetric error of an SLM part will result in poor part accuracy, especially for FGs with higher MADRs. Therefore, a build orientation is crucial to minimize the weighted volumetric error.

(2) Surface roughness model. Surface roughness is a popular indicator for measuring the surface quality of an AM part [13,19–21]. Past studies have investigated the effects of the process parameters and orientation on the surface roughness of the SLM parts [13,55–61]. A suitable and reasonable prediction model of the surface roughness for an SLM part is essential in practical application. However, in the publications, prediction models are either not given [56–58] or are not applicable due to complexity [55,59,61]. Accordingly, the prediction model proposed by Brika et al. [13] is applied in this study. However, it is simple and cannot insufficiently reflect the effects of the process parameters and orientation on the surface roughness. This model was developed based on a study of the surface roughness of SLM Ti–6Al–4V samples for the up-facing and side-facing surfaces in different build orientations with a constant layer thickness of 0.03 mm. The surface roughness Ra_i^{f} of the ith facet F_i for an angle α_i is estimated based on polynomial regression, which is expressed as follows [13,42]:

$$Ra_i^{\mathrm{f}} = 9.4148 + 0.0389 |90 - \alpha_i|. \tag{3}$$

The average surface roughness, Ra_{asr}, of an SLM part is calculated by [13,19,42]

$$Ra_{\mathrm{asr}} = \frac{\sum_{i=1}^{n_{\mathrm{f}}} Ra_i^{\mathrm{f}} A_i^{\mathrm{f}}}{\sum_{i=1}^{n_{\mathrm{f}}} A_i^{\mathrm{f}}}. \tag{4}$$

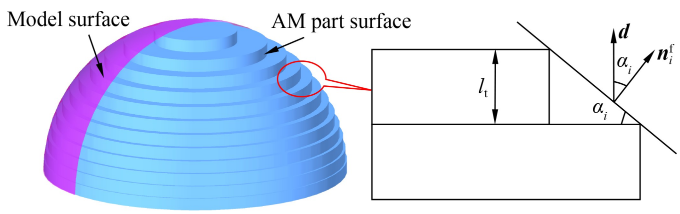

Fig. 3 Illustration of the volumetric error in additive manufacturing (AM).

In Refs. [13,42], Eq. (3) was suitable for the up-facing and downward-facing facets (also known as overhang facets). The support structure is essential for the overhang facets to improve their surface quality [2], and the support removal process damages the surface quality of the overhang facets of an SLM part [56]. To this end, the Ra value of a supported facet is weighted as

$$Ra_i^{\mathrm{fs}} = (1+\sigma)(9.4148+0.0389\,|90-\alpha_i|), \tag{5}$$

where Ra_i^{fs} is the surface roughness of the ith supported facet, and σ is the weight for the surface roughness calculation of a supported facet. The value of σ was set as 0.2 for FDM based on experiments in Ref. [19]. However, similar experiments for SLM are unavailable. Given that the layer thickness of the SLM is smaller than the FDM, σ is set as 0.1 for SLM.

Thus, the estimation model of the average surface roughness for an SLM part is given by

$$Ra_{\mathrm{asr}} = \frac{\sum_{j=1}^{n_{\mathrm{f}}^{\mathrm{n}}} Ra_j^{\mathrm{f}} A_j^{\mathrm{f}} + \sum_{k=1}^{n_{\mathrm{f}}^{\mathrm{s}}} Ra_k^{\mathrm{fs}} A_k^{\mathrm{f}}}{\sum_{i=1}^{n_{\mathrm{f}}} A_i^{\mathrm{f}}}, \tag{6}$$

where $n_{\mathrm{f}}^{\mathrm{n}}$ and $n_{\mathrm{f}}^{\mathrm{s}}$ are the numbers of the facets without and with supports, respectively, and $n_{\mathrm{f}} = n_{\mathrm{f}}^{\mathrm{n}} + n_{\mathrm{f}}^{\mathrm{s}}$.

Similar to the volumetric error model, the weighted average surface roughness, Ra_{wasr}, of an SLM part can be achieved by

$$Ra_{\mathrm{wasr}} = \sum_{i=1}^{n_{\mathrm{fg}}} w_i^{\mathrm{fg}} Ra_{\mathrm{asr},i}, \tag{7}$$

where $Ra_{\mathrm{asr},i}$ is the average surface roughness of the ith FG obtained by Eq. (6).

The higher the value of Ra_{wasr} is, the worse the surface quality of an SLM part will be. A build orientation is crucial to minimize the weighted average surface roughness.

(3) Support volume model. The support volume is an essential objective because it affects the build time and cost. Once the overhang angle of a facet is greater than the threshold (the threshold is 45° in this study), the support structure is required for it [2,17]. The ray–triangle intersection method [62] is applied to estimate the support volume with desirable computation efficiency. As shown in Fig. 4, the projection of the bounding box of a model on the platform is first partitioned into numerous small square grids (Fig. 4(b)). The ray of each grid is constructed from the grid's center and upward along the build direction and used to intersect with the model's triangles. The number of grids is controlled by the edge length of the grid as follows:

$$n_{\mathrm{g}}^{x} = \mathrm{round}\left(\frac{B_{\mathrm{length}}}{l_{\mathrm{e}}}\right), \tag{8}$$

$$n_{\mathrm{g}}^{y} = \mathrm{round}\left(\frac{B_{\mathrm{width}}}{l_{\mathrm{e}}}\right), \tag{9}$$

where n_{g}^{x} and n_{g}^{y} are the numbers of the grids along the x- and y-axis, respectively, B_{length} and B_{width} are the length and width of the part's bounding box along the x- and

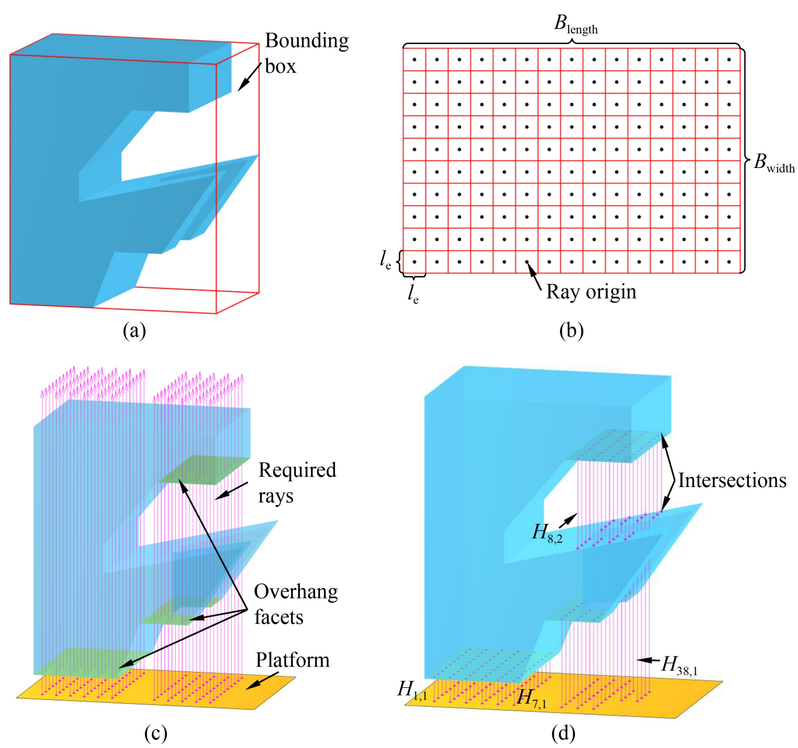

Fig. 4 Illustration of support volume estimation: (a) manifold mesh model, (b) grids and ray origins, (c) required rays intersected with the overhang facets, and (d) support segments.

y-axis, respectively, and l_e is the edge length of the grid. The number of the grids is $n_g = n_g^x \times n_g^y$.

The value of l_e is related to the part size. Then, the overhang facets of the model are detected and applied to obtain the intersected rays, as shown in Fig. 4(c).

The intersection in a supported facet and the closest intersection downward along the ray will construct a segment (Fig. 4(d)). The support volume of each grid can be obtained by summing the products of the grid area and segments, which can be expressed as follows:

$$V_i^g = A_g \sum_j H_{i,j}, \tag{10}$$

where V_i^g is the support volume of the ith grid, $A_g = l_e^2$ is the area of the grid generated in the projection of the bounding box on the platform, and $H_{i,j}$ is the height of the jth segment of the ith supported ray. Accordingly, the support volume, V_s, of an SLM part can be determined as

$$V_s = \sum_{i=1}^{n_r} \left(l_e^2 \sum_j H_{i,j} \right), \tag{11}$$

where n_r is the number of the rays intersected with the overhang facets.

Finding a build orientation is essential to minimize the entire support volume of an SLM part.

(4) Build time model. Build time is likewise an essential objective in SLM and influences the build cost of a part. It is the sum of the building time and the preparation time (i.e., recoating time between two adjacent layers of each layer). On the basis of Refs. [13,22,42], the entire build time, T_b, of an SLM part can be estimated by

$$T_b = \frac{H_p + H_{pp}}{l_t} T_r + \frac{V_p}{R_b^p} + \frac{V_s}{R_b^s}, \tag{12}$$

where H_p is the part's height, H_{pp} is the height between the part and the platform, T_r is the recoating time of each layer, V_p is the part volume, and R_b^p and R_b^s are the build rates of the part and support, respectively. The part's build rate is defined by

$$R_b^p = l_t v_s H_d^p, \tag{13}$$

where v_s is the laser scanning speed, and H_d^p is the hatch distance for filling the part. As shown in Fig. 5, one layer's laser scanning path comprises contour, filling, and support; and H_d^s is the hatch distance of the lattice support structure. In Fig. 5, the green triangle and square represent the start and end points of the contour path, respectively. The red triangle and square represent the start and end points of the filling path, respectively. The purple triangle and square represent the start and end points of the support path, respectively.

The build rate R_b^s of the support can be the same as R_b^p, and the resulting support structure is then completely solid. In practice, the lattice support structure is commonly applied to reduce the material used and build cost in SLM [14,63]. The lattice support structure is constructed by a set of cell blocks, and H_d^s is greater than H_d^p. Thus, the support's build rate is defined by

$$R_b^s = \frac{l_t v_s H_d^s}{2}. \tag{14}$$

A build orientation is essential to minimize the entire build time of an SLM part.

(5) Build cost model. Build cost is a critical indicator in SLM, mainly due to the use of high-quality metal powder. The build cost, C_{build}, of an SLM part is composed of material, energy, and indirect costs [13], which can be expressed as

$$C_{build} = C_{material} + C_{energy} + C_{indirect}, \tag{15}$$

where $C_{material}$ is the material cost, C_{energy} is the energy cost, and $C_{indirect}$ is the indirect cost.

$C_{material}$ is composed of the material cost used for the part, support structure, and wasted material during the fabrication, which can be expressed as follows:

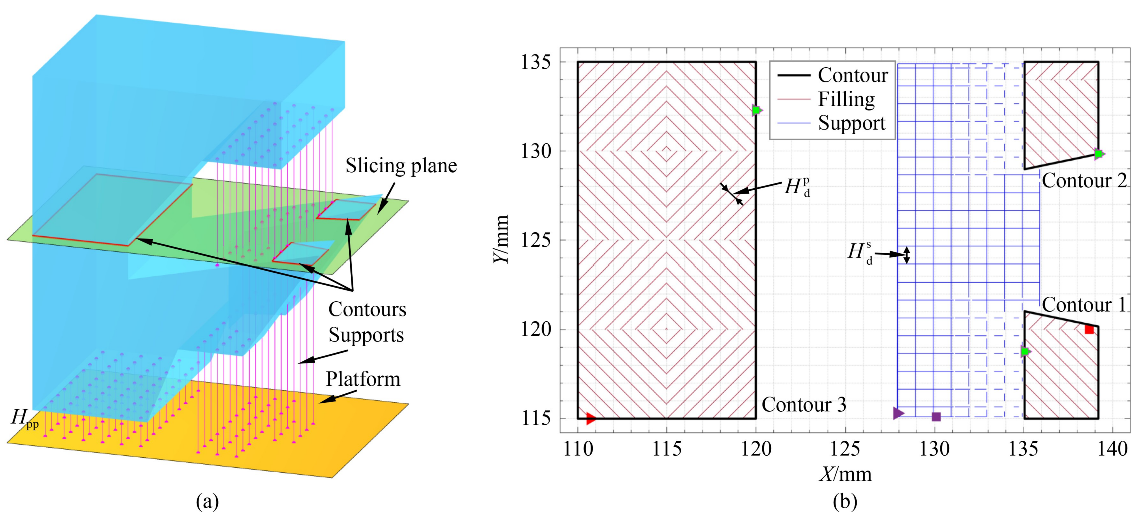

Fig. 5 Illustration of the model slicing and the laser scanning path: (a) model slicing and (b) laser scanning path.

$$C_{\mathrm{material}} = (V_{\mathrm{p}} + S_{\mathrm{density}} V_{\mathrm{s}}) M_{\mathrm{density}} M_{\mathrm{porosity}} P_{\mathrm{material}} (1 + R_{\mathrm{waste}}), \tag{16}$$

where M_{density} and M_{porosity} are the density and porosity of the material, respectively, P_{material} is the material price, R_{waste} is the material waste rate, and S_{density} is the volume fraction of the lattice support structure [14,64].

C_{energy} is given by

$$C_{\mathrm{energy}} = (V_{\mathrm{p}} + S_{\mathrm{density}} V_{\mathrm{s}}) M_{\mathrm{density}} M_{\mathrm{porosity}} E_{\mathrm{consumption}} P_{\mathrm{energy}}, \tag{17}$$

where $E_{\mathrm{consumption}}$ is the energy consumption rate, and P_{energy} is the energy price.

C_{indirect} is written as

$$C_{\mathrm{indirect}} = T_{\mathrm{b}} R_{\mathrm{indirect}} \frac{B_{\mathrm{length}} B_{\mathrm{width}}}{A_{\mathrm{platform}}}, \tag{18}$$

where R_{indirect} is the indirect cost rate, and A_{platform} is the area of the fabrication platform.

The build cost of an SLM part should be reduced by selecting an appropriate build orientation.

3.2.2 Determination of weights using FAHP

The weights of different FGs in the estimation models of volumetric error and surface roughness are related to the MADRs. An FG with a high MADR should match a high weight [41]. The weights can be assigned manually. However, human judgment is often fuzzy in real life. For this, the extent FAHP method [49] is applied to determine the weights of the FGs. FAHP uses linguistic variables to express the relative importance of different objectives by pairwise comparison. The linguistic variable can be scaled by a triangular fuzzy number (TFN).

A TFN $\widetilde{A} = (l, m, u)$ is a fuzzy set, the probability of a real value, x, belong to $\widetilde{A}$ can be determined by the membership function, $\mu_{\widetilde{A}}(x)$, of $\widetilde{A}$, which is given by

$$\mu_{\widetilde{A}}(x) = \begin{cases} \dfrac{x-l}{m-l}, & l \leqslant x \leqslant m, \\ \dfrac{u-x}{u-m}, & m \leqslant x \leqslant u, \\ 0, & \text{otherwise,} \end{cases} \tag{19}$$

where $0 < l \leqslant m \leqslant u$, l and u are the lower and upper bounds of a TFN, respectively, and m denotes the most promising value of a TFN (i.e., $\mu_{\widetilde{A}}(m) = 1$).

The linguistic variables scaled by the TFNs are presented in Table 1 [51].

The FAHP method obeys the following steps [51]:

(1) The value of the fuzzy synthetic extent, $S_i = (l_{S_i}, m_{S_i}, u_{S_i})$, concerning the ith object g_i is defined by

$$S_i = \sum_{j=1}^{q} M_{g_i}^j \times \left[\sum_{i=1}^{n} \sum_{j=1}^{q} M_{g_i}^j\right]^{-1}, \tag{20}$$

where $M_{g_i}^j = (l_{g_i}^j, m_{g_i}^j, u_{g_i}^j)$ is a TFN and is the extent analysis value of the jth factor to the ith object in the fuzzy judgment matrix, $\boldsymbol{M}_{n\times q}$, n is the number of objects, and $\sum_{j=1}^{q} M_{g_i}^j$ is obtained by

Table 1 TFNs for linguistic variables [51]

Linguistic variables	TFN	Scale of TFN
Equal importance	1	(1, 1, 1)
Little importance	$\widetilde{1}$	(1, 1, 3)
Intermediate value between $\widetilde{1}$ and $\widetilde{3}$	$\widetilde{2}$	(1, 2, 4)
Moderate importance	$\widetilde{3}$	(1, 3, 5)
Intermediate value between $\widetilde{3}$ and $\widetilde{5}$	$\widetilde{4}$	(2, 4, 6)
Essential importance	$\widetilde{5}$	(3, 5, 7)
Intermediate value between $\widetilde{5}$ and $\widetilde{7}$	$\widetilde{6}$	(4, 6, 8)
Extreme importance	$\widetilde{7}$	(5, 7, 9)
Intermediate value between $\widetilde{7}$ and $\widetilde{9}$	$\widetilde{8}$	(6, 8, 10)
Absolute importance	$\widetilde{9}$	(7, 9, 11)

$$\sum_{j=1}^{q} M_{g_i}^j = \left(\sum_{j=1}^{q} l_{g_i}^j, \sum_{j=1}^{q} m_{g_i}^j, \sum_{j=1}^{q} u_{g_i}^j\right), \tag{21}$$

where q is the number of factors of one object, and $\left[\sum_{i=1}^{n} \sum_{j=1}^{q} M_{g_i}^j\right]^{-1}$ is obtained by

$$\left[\sum_{i=1}^{n} \sum_{j=1}^{q} M_{g_i}^j\right]^{-1} = \left(\frac{1}{\sum_{i=1}^{n} \sum_{j=1}^{q} u_{g_i}^j}, \frac{1}{\sum_{i=1}^{n} \sum_{j=1}^{q} m_{g_i}^j}, \frac{1}{\sum_{i=1}^{n} \sum_{j=1}^{q} l_{g_i}^j}\right). \tag{22}$$

Thereby, S_i can be given by

$$S_i = \left(\frac{\sum_{j=1}^{q} l_{g_i}^j}{\sum_{i=1}^{n} \sum_{j=1}^{q} u_{g_i}^j}, \frac{\sum_{j=1}^{q} m_{g_i}^j}{\sum_{i=1}^{n} \sum_{j=1}^{q} m_{g_i}^j}, \frac{\sum_{j=1}^{q} u_{g_i}^j}{\sum_{i=1}^{n} \sum_{j=1}^{q} l_{g_i}^j}\right). \tag{23}$$

(2) The degree of possibility of $S_2 = (l_{S_2}, m_{S_2}, u_{S_2}) \geqslant S_1 = (l_{S_1}, m_{S_1}, u_{S_1})$ is defined as

$$V(S_2 \geqslant S_1) = \mathrm{Sup}_{y \geqslant x} \min(\mu_{S_2}(y), \mu_{S_1}(x)), \tag{24}$$

where S_2 and S_1 are obtained by Eq. (20), then Eq. (24) can be equivalently expressed as follows:

$$V(S_2 \geqslant S_1) = \mathrm{hgt}(S_2 \cap S_1) = \mu_{S_2}(d), \tag{25}$$

$$\mu_{S_2}(d) = \begin{cases} 1, & m_{S_2} \geqslant m_{S_1}, \\ 0, & l_{S_1} \geqslant u_{S_2}, \\ \dfrac{l_{S_1} - u_{S_2}}{(m_{S_2} - u_{S_2}) - (m_{S_1} - l_{S_1})}, & \text{otherwise,} \end{cases} \tag{26}$$

where d is the ordinate of the highest intersection point D between μ_{S_1} and μ_{S_2}. The values of $V(S_2 \geqslant S_1)$ and $V(S_1 \geqslant S_2)$ are needed to compare S_2 and S_1.

(3) The degree of possibility for a convex fuzzy number S to be greater than k convex fuzzy numbers S_i $(i = 1, 2, ..., k)$ is defined by

$$\begin{aligned} &V(S \geqslant S_1, S_2, ..., S_k) \\ &= V[(S \geqslant S_1) \cap (S \geqslant S_2) \cap \cdots \cap (S \geqslant S_k)] \\ &= \min V(S \geqslant S_i),\ i = 1, 2, ..., k. \end{aligned} \tag{27}$$

(4) The normalized non-fuzzy weight vector can be expressed as

$$\boldsymbol{W} = (d(S_1), d(S_2), ..., d(S_n)), \tag{28}$$

where $d(S_i)$ is the weight of the ith object, and is given by

$$d(S_i) = \frac{d'(S_i)}{\sum_{i=1}^{n} d'(S_i)}, \tag{29}$$

where $d'(S_i)$ is calculated according to Eq. (27), and written as

$$d'(S_i) = \min V(S_i \geqslant S_t), \text{ for } t = 1, 2, ..., n,\ t \neq i. \tag{30}$$

3.2.3 Many-objective optimization

The MOO generates the ABOs regarding the considered objectives. The part's rotation angles (θ_x, θ_y) around the x- and y-axis will define an ABO. Accordingly, θ_x and θ_y are taken as the decision variables. The rotation angle around the z-axis is not considered because it does not affect SLM manufacturing. The proposed MOO problem can be formulated as

$$\begin{cases} \text{Minimize} & \{f_1(\theta_x, \theta_y), f_2(\theta_x, \theta_y), ..., f_{n_o}(\theta_x, \theta_y)\}, \\ \text{subject to} & 0° \leqslant \theta_x \leqslant 180°, \\ & 0° \leqslant \theta_y \leqslant 180°, \end{cases} \tag{31}$$

where $f_i(\theta_x, \theta_y)$ represents the estimation model function of the ith objective, and n_o is the number of considered objectives.

The ranges of θ_x and θ_y will make all the orientations in the 3D space covered. Equation (29) can be solved in two ways. One is to apply the WSM [13,34], which can be formulated as

$$F_{\text{wsm}} = \sum_{i=1}^{n_o} w_i^o \frac{OV_i - OV_i^{\min}}{OV_i^{\max} - OV_i^{\min}}, \tag{32}$$

where w_i^o and OV_i are the weight and value of the ith objective, respectively, and $OV_i^{\max}$ and $OV_i^{\min}$ are the maximum and minimum values of the ith objective, respectively. The WSM is simple and efficient in solving the MOO problem and generates only one solution.

The other one is applying the Pareto-based optimization to obtain the Pareto front of the MOO problem [19,24,27,38], which will generate a set of Pareto optimal solutions. The final optimal solution can be selected from those solutions by the decision maker. In comparison with the WSM, the Pareto-based optimization can better reflect the characteristics of individual objectives.

This study adopts the NSGA-II with vectorized calculation provided by the MATLAB software to generate the Pareto ABOs. It supports the vectorized calculation to speed up the solving process. The volumetric error, surface roughness, and build time and cost models are easily coded in vectorized format. The support volume model is more complex but can be vectorized partly. To maintain the population diversity, the population size and the maximum generation are set to 100 and 600, respectively. The number of optimal solutions in the Pareto front is set to be the same as the population size, and the other parameters are kept the same as the default values.

3.3 OBO determination

The obtained ABOs are equivalently optimum, referring to Pareto optimality. An OBO should be selected from the ABOs in practice. The OBO determination is an MODM problem and can be summarized as a decision matrix, ***DM***, as shown as follows:

$$\boldsymbol{DM} = \begin{bmatrix} x_{1,1} & x_{1,2} & \cdots & x_{1,n} \\ x_{2,1} & x_{2,2} & \cdots & x_{2,n} \\ \vdots & \vdots & \ddots & \vdots \\ x_{m,1} & x_{m,2} & \cdots & x_{m,n} \end{bmatrix}, \tag{33}$$

where $x_{i,j}$ is the value of the jth objective for the ith ABO.

A weight vector that will reflect the relative importance of the considered objectives is given by

$$\boldsymbol{W}_o = [w_1^o, w_2^o, ..., w_n^o], \tag{34}$$

where $w_j^o > 0$ is the jth objective weight, and $\sum_{j=1}^{n} w_j^o = 1$.

The objective weights are crucial because it directly affects the OBO determination. Most of the existing works have defined the weights manually. Nevertheless, specifying the proper objective weights is challenging [17]. Therefore, the objective weights are also determined by the FAHP.

This study integrates the TOPSIS and CSM methods [50] to solve the proposed MODM problem. The best alternative determined by the TOPSIS will have the minimum distance to the positive ideal solution and maximum distance to the negative ideal solution, which was likewise utilized in Ref. [24]. Nonetheless, the TOPSIS only considers the distance metric and can induce several alternatives with the same measured distance in the high-dimensional solution space. Consequently, the CSM is applied to distinguish the alternatives with the same measured distance. The CSM measures the similarity of two vectors by the cosine of the angle between them. The greater the cosine is, the more similar the two vectors will be. It pays more attention to the direction rather than the distance and is sensitive to even a tiny deformation. The OBO should have the highest CMS with the positive ideal solution.

The TOPSIS method is described in the following steps:

(1) Normalize the decision matrix of ***DM*** as follows:

$$r_{i,j} = \frac{x_{i,j}}{\sqrt{\sum_{i=1}^{m} x_{i,j}^2}},\ i = 1, 2, ..., m,\ j = 1, 2, ..., n. \tag{35}$$

(2) Calculate the weighted normalized decision matrix as follows:

$$v_{i,j} = w_j^o r_{i,j},\ i = 1, 2, ..., m,\ j = 1, 2, ..., n. \tag{36}$$

(3) Determine the positive ideal solution A^+ and negative ideal solution A^- as follows:

$$A^+ = (v_1^+, v_2^+, ..., v_n^+), \tag{37}$$

$$A^- = (v_1^-, v_2^-, ..., v_n^-). \tag{38}$$

If the jth objective is a benefit objective, then $v_j^+ = \max\{v_{1,j}, v_{2,j}, ..., v_{m,j}\}$ and $v_j^- = \min\{v_{1,j}, v_{2,j}, ..., v_{m,j}\}$. If the jth objective is a cost objective, then $v_j^+ = \min\{v_{1,j}, v_{2,j}, ..., v_{m,j}\}$ and $v_j^- = \max\{v_{1,j}, v_{2,j}, ..., v_{m,j}\}$.

(4) Calculate the distances D_i^+ and D_i^- from each alternative to A^+ and A^-, respectively, as follows:

$$D_i^+ = \sqrt{\sum_{j=1}^{n}\left(v_{i,j} - v_j^+\right)^2},\ i = 1, 2, ..., m, \tag{39}$$

$$D_i^- = \sqrt{\sum_{j=1}^{n}\left(v_{i,j} - v_j^-\right)^2},\ i = 1, 2, ..., m. \tag{40}$$

(5) Calculate the relative closeness to the ideal solution as follows:

$$C_i = \frac{D_i^-}{D_i^+ + D_i^-}. \tag{41}$$

(6) Rank the alternatives following C_i ($0 \leqslant C_i \leqslant 1$). The greater C_i is, the better alternative will be.

To utilize the CSM method, Steps 1–3 of the TOPSIS method are likewise applied. Then, the CSM, M_i, between each alternative and A^+ is defined as

$$M_i = \frac{\sum_{j=1}^{n}\left(v_{i,j} v_j^+\right)}{\sqrt{\sum_{j=1}^{n} v_{i,j}^2}\sqrt{\sum_{j=1}^{n} (v_j^+)^2}}. \tag{42}$$

The greater M_i is, the more similar the alternative to the positive ideal solution will be. Given that C_i and M_i have the same positive influence, the integration value, IV_i, of the TOPSIS and CSM can be expressed as

$$IV_i = \rho C_i' + (1-\rho) M_i', \tag{43}$$

where ρ ($0 \leqslant \rho \leqslant 1$) is a coefficient to adjust the relative importance of the TOPSIS and CSM, here, ρ is set as 0.5, which indicates that the importance of TOPSIS and CSM is the same, C_i' and M_i' are the normalized values of C_i and M_i, respectively, and given as follows:

$$C_i' = \frac{C_i}{\sum_{i=1}^{m} C_i}, \tag{44}$$

$$M_i' = \frac{M_i}{\sum_{i=1}^{m} M_i}. \tag{45}$$

The greater IV_i is, the better the alternative will be. In comparison with the TOPSIS method, the proposed integrated MODM method that selects the OBO not only has the highest relative closeness between the positive and negative ideal solutions but also the highest similarity to the positive ideal solution.

4 Applications and discussion

4.1 Case studies

Two MFMPs are applied to illustrate the proposed method, and the detailed geometric information is presented in Table 2. Figure 6 depicts the manifold mesh models of the two MFMPs with their original orientation. The relevant process parameters used for the objective estimation models are provided in Table 3. In Table 3, the layer thickness, recoating time, laser scanning speed, and

Table 2 Geometric information of the two MFMPs

MFMP	Length/ mm	Width/ mm	Height/ mm	Volume/ mm^3	Area/ mm^2
Connecting rod	53.58	26.92	25.99	10236.77	5360.21
Bracket	63.00	46.78	60.13	17644.09	9573.85

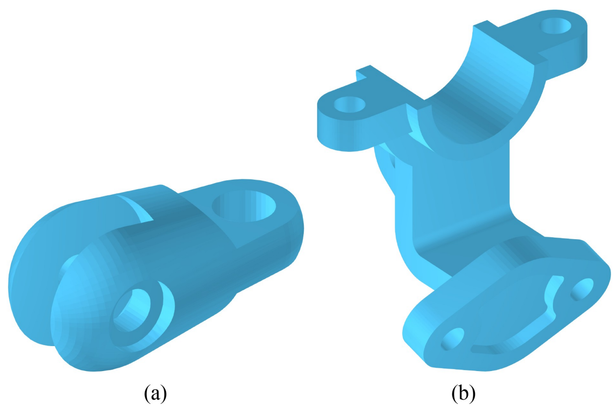

Fig. 6 Manifold mesh models of the two multi-feature mechanical parts: (a) connecting rod and (b) bracket.

Table 3 SLM process parameters used for the objective estimation models

Parameter	Value
l_t	0.03 mm
T_r	20 s
v_s	1250 mm/s
H_d^p	0.07 mm
H_d^s	1 mm
H_{pp}	3 mm
$M_{density}$	4.43 g/cm^3
$M_{porosity}$	99.5%
R_{waste}	0.1
$S_{density}$	0.3
$P_{material}$	300 USD/kg
P_{energy}	0.18 USD/(kW·h)
$E_{consumption}$	162.13 kW·h/kg
$R_{indirect}$	53.35 USD/h
$A_{platform}$	62500 mm^2

hatch spacing are cited from Ref. [13]; the hatch distance of the lattice structure is cited from Ref. [63]; and the fraction of the support volume is cited from Ref. [14].

Figure 7(a) presents the 13 recognized features of the connecting rod with different colors. Three FGs are obtained for the connecting rod following its MADRs, and the features of an FG have the same color, as presented in Fig. 7(b). The feature numbers of the three FGs for the connecting rod are 5, 4, and 4. Figure 8(a) presents the 31 features of the bracket with different colors. There exist four FGs following the MADRs, as illustrated in Fig. 8(b). The feature numbers of the four FGs for the bracket are 3, 5, 2, and 21.

Notably, as the MADR increases, the machining cost becomes increasingly high. Accordingly, the FG's importance should increase with the MADR's increment. Depending on the MADRs of the connecting rod, the pairwise fuzzy judgment matrix, $\boldsymbol{Q}_1^{\mathrm{fg}}$, and ultimate weight vector, $\boldsymbol{W}_1^{\mathrm{fg}}$, of the FGs obtained by the FAHP are expressed as follows:

$$\boldsymbol{Q}_1^{\mathrm{fg}} = \begin{pmatrix} (1,\ 1,\ 1) & (1,\ 2,\ 4) & (2,\ 4,\ 6) \\ (1/4,\ 1/2,\ 1) & (1,\ 1,\ 1) & (1,\ 2,\ 4) \\ (1/6,\ 1/4,\ 1/2) & (1/4,\ 1/2,\ 1) & (1,\ 1,\ 1) \end{pmatrix},$$

$$\boldsymbol{W}_1^{\mathrm{fg}} = (0.5293,\ 0.3541,\ 0.1166)^{\mathrm{T}}.$$

Similarly, the pairwise fuzzy judgment matrix and ultimate weight vector of the FGs for the bracket are obtained as follows:

$$\boldsymbol{Q}_2^{\mathrm{fg}} = \begin{pmatrix} (1,\ 1,\ 1) & (1,\ 3,\ 5) & (2,\ 4,\ 6) & (3,\ 5,\ 7) \\ (1/5,\ 1/3,\ 1) & (1,\ 1,\ 1) & (1,\ 2,\ 4) & (1,\ 3,\ 5) \\ (1/6,\ 1/4,\ 1/2) & (1/4,\ 1/2,\ 1) & (1,\ 1,\ 1) & (1,\ 1,\ 3) \\ (1/7,\ 1/5,\ 1/3) & (1/5,\ 1/3,\ 1) & (1/3,\ 1,\ 1) & (1,\ 1,\ 1) \end{pmatrix},$$

$$\boldsymbol{W}_2^{\mathrm{fg}} = (0.4705,\ 0.3224,\ 0.1550,\ 0.0521)^{\mathrm{T}}.$$

Once the weights of the FGs are determined, the Pareto ABOs can be achieved. For that, the relevant optimization objectives should be identified first. The volumetric error, surface roughness, support volume, and build time are selected for the connecting rod. Given that four optimization objectives exist, the Pareto front cannot easily be depicted in a single graph. To reflect the considered objectives' trade-offs, any three of the four objectives in the Pareto front are shown in a single graph, which will generate four graphs. Figure 9 presents the Pareto front of the connecting rod. Ra_{wasr} in the Pareto

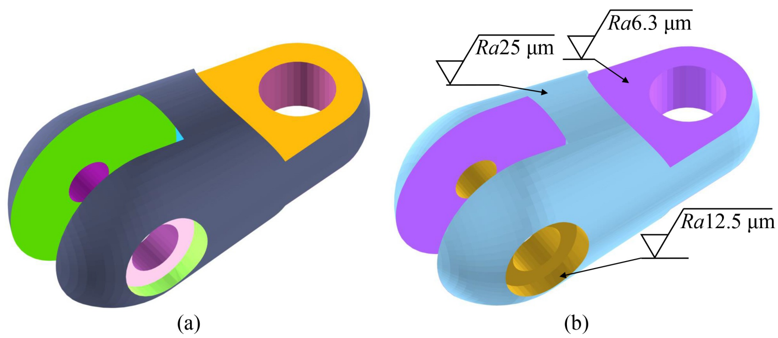

Fig. 7 Features and feature groups of the connecting rod: (a) features and (b) feature groups.

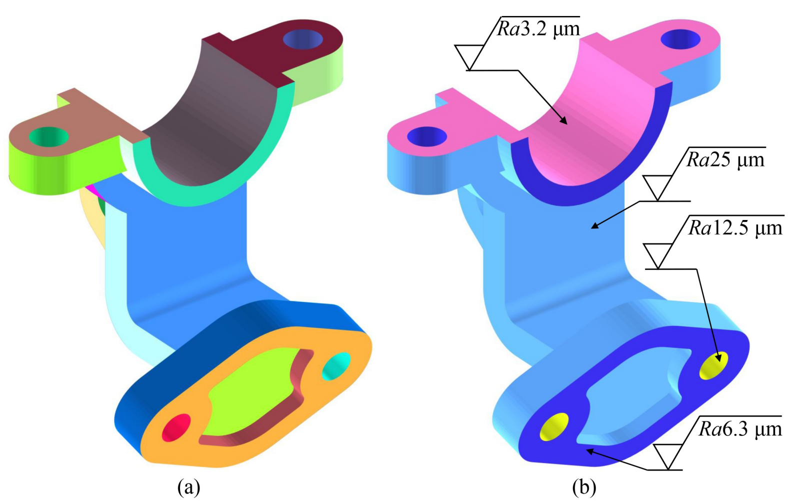

Fig. 8 Features and feature groups of the bracket: (a) features and (b) feature groups.

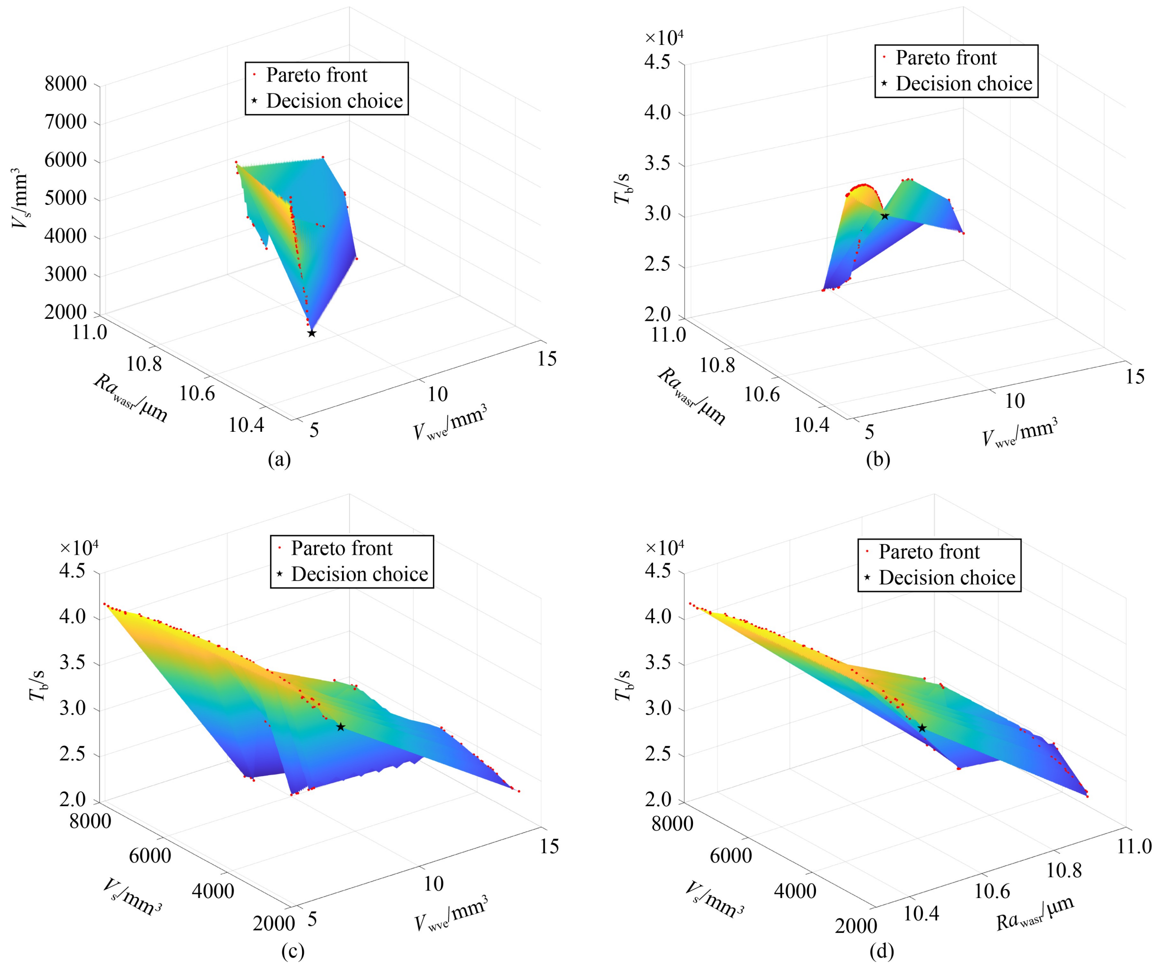

Fig. 9 Pareto front of the four objectives for the connecting rod: (a) V_{wve}, Ra_{wasr}, and V_s, (b) V_{wve}, Ra_{wasr}, and T_b, (c) V_{wve}, V_s, and T_b, and (d) Ra_{wasr}, V_s, and T_b.

front changes a little, whereas the other three objectives' values have sufficient changes, especially for V_s and T_b.

The weights of the four objectives should be obtained through the FAHP first to achieve an OBO. Indeed, the pairwise fuzzy comparison matrix for the four objectives can be directly constructed by the decision maker's preferences. However, it should likewise reflect the inherent relationship between each objective and the OBO. Given that the change of Ra_{wasr} is extremely small, using it to distinguish the difference between the ABOs is difficult. Thus, Ra_{wasr} has a little effect on the OBO. V_{wve} reflects the part accuracy and has a sufficient distinction, as shown in Fig. 9. In comparison with other objectives, V_{wve} should have a higher weight in the OBO determination. The presence of the supports will increase the build cost and time, and the support removal will damage the surface quality. As a result, V_s is more crucial than Ra_{wasr}. The build time can adopt the same importance as the support volume. The fuzzy pairwise comparison matrix, $\boldsymbol{Q}_o$, of the four objectives for the connecting rod can be considered as follows:

$$\boldsymbol{Q}_o = \begin{pmatrix} (1,\ 1,\ 1) & (1,\ 3,\ 5) & (1,\ 2,\ 4) & (1,\ 2,\ 4) \\ (1/5,\ 1/3,\ 1) & (1,\ 1,\ 1) & (1/4,\ 1/2,\ 1) & (1/4,\ 1/2,\ 1) \\ (1/4,\ 1/2,\ 1) & (1,\ 2,\ 4) & (1,\ 1,\ 1) & (1,\ 1,\ 1) \\ (1/4,\ 1/2,\ 1) & (1,\ 2,\ 4) & (1,\ 1,\ 1) & (1,\ 1,\ 1) \end{pmatrix}.$$

The correspondence weight vector is $\boldsymbol{W}_o = (0.3529, 0.1443, 0.2514, 0.2514)^T$. Then, applying the integrated MODM method will achieve the decision choice (marked as a black star; i.e., the OBO), from the Pareto front of the connecting rod, as shown in Fig. 9.

The build cost is influenced by the support volume and build time simultaneously. To present the effects of different objectives on the build orientation, the build time objective used in the connecting rod is replaced by the build cost to generate the Pareto ABOs for the bracket. Figure 10 illustrates the obtained Pareto front and the OBO of the bracket, in which the objective weights are the same as that of the connecting rod.

The OBOs of the connecting rod and bracket are (0.2563°, 45.1261°) and (89.5595°, 135.0014°), respectively, which are presented in Fig. 11. The objective values of the original orientations and OBOs for

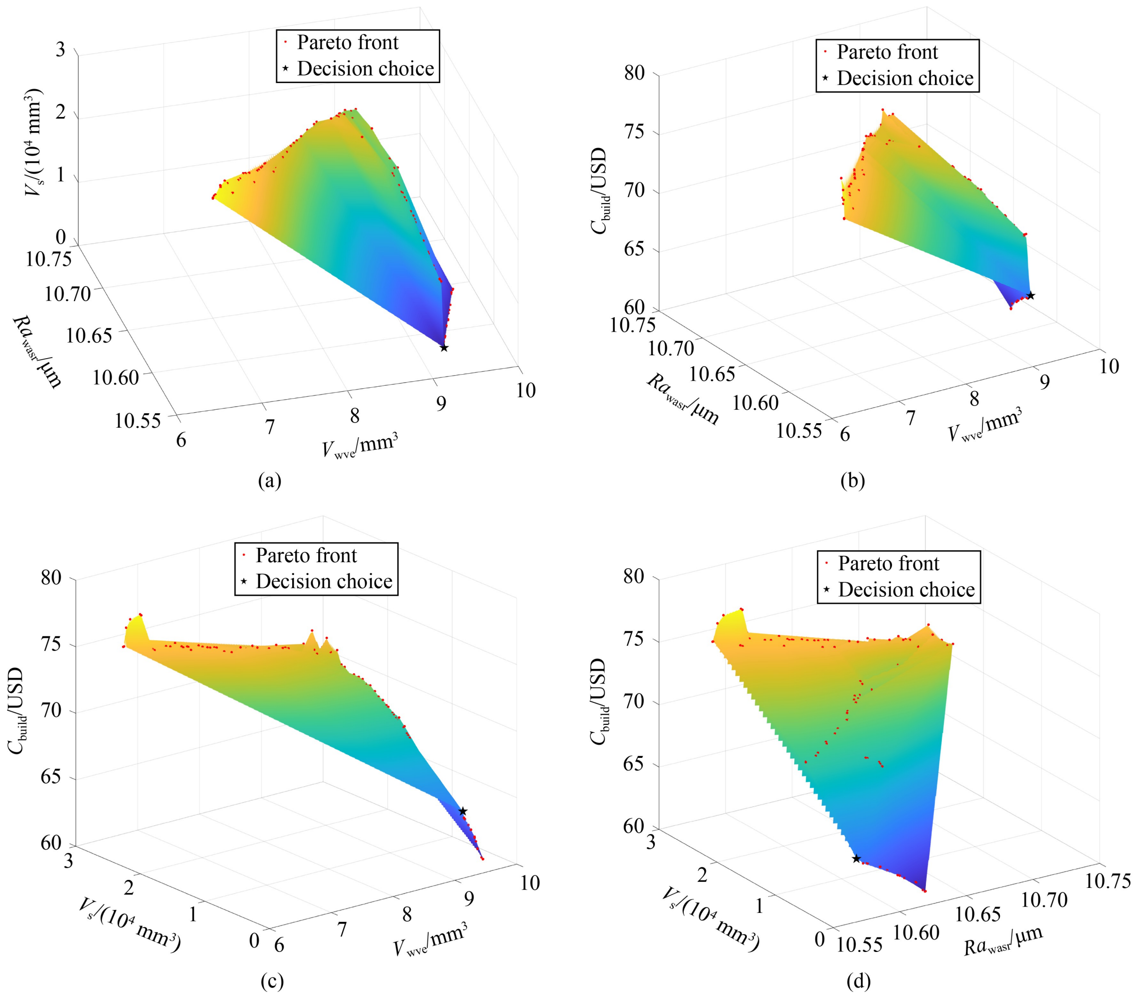

Fig. 10 Pareto front of the four objectives for the bracket: (a) V_{wve}, Ra_{wasr}, and V_s, (b) V_{wve}, Ra_{wasr}, and C_{build}, (c) V_{wve}, V_s, and C_{build}, and (d) Ra_{wasr}, V_s, and C_{build}.

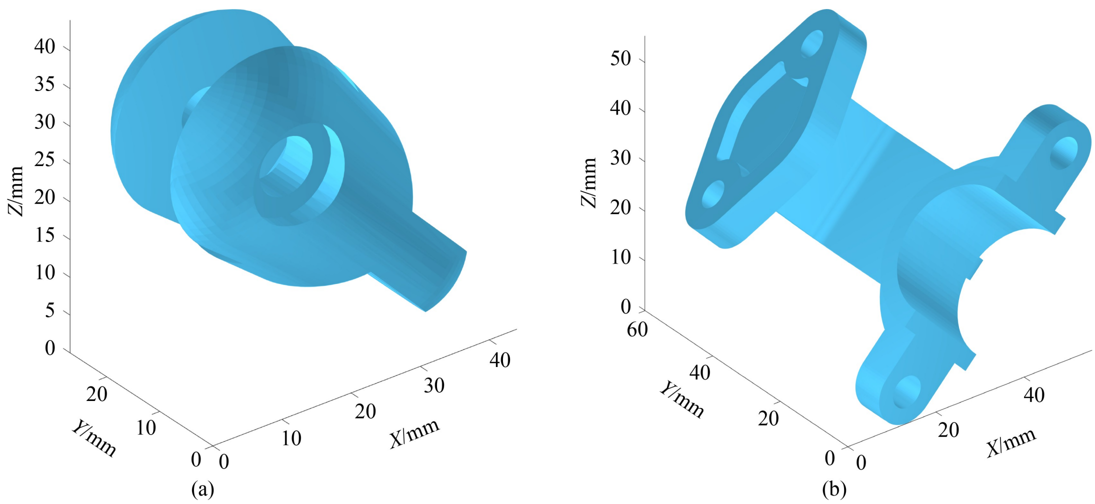

Fig. 11 Optimal build orientations for the connecting rod and bracket: (a) connecting rod and (b) bracket.

the two MFMPs are listed in Tables 4 and 5, respectively. The results suggest that the proposed method optimizes the first three objectives for the connecting rod compared with the original orientation; significantly, the support volume decreases by 53.43%, whereas the build time increases by 50.43%. The proposed method optimizes all

Table 4 Comparison of the original orientation and OBO for the connecting rod

Orientation	$V_{\mathrm{wve}}/\mathrm{mm}^3$	$Ra_{\mathrm{wasr}}/\mu\mathrm{m}$	$V_{\mathrm{s}}/\mathrm{mm}^3$	$T_{\mathrm{b}}/\mathrm{s}$	IV
Original	8.1129	10.8011	6041.0644	23547.7393	0.00970
OBO	7.8981	10.5099	2836.6676	35423.6799	0.01137

Table 5 Comparison of the original orientation and OBO for the bracket

Orientation	$V_{\mathrm{wve}}/\mathrm{mm}^3$	$Ra_{\mathrm{wasr}}/\mu\mathrm{m}$	$V_{\mathrm{s}}/\mathrm{mm}^3$	$C_{\mathrm{build}}/\mathrm{USD}$	IV
Original	9.6181	10.9872	39258.6953	82.1573	0.00414
OBO	9.2628	10.5730	1292.4769	64.5985	0.01297

the four objectives for the bracket compared with the original orientation; especially, the support volume decreases by 96.71%. The objective values in the original orientation are added to the Pareto front to demonstrate the OBO's effectiveness. The proposed integrated MODM method is applied to evaluate them, and the corresponding results (IV) for the connecting rod and bracket are listed in Tables 4 and 5, respectively. Given that the IV value of the OBO is greater than that of the original orientation, the obtained OBOs of the connecting rod and bracket are effective solutions.

4.2 Effectiveness comparison

The accuracy of the estimation models of the objectives considered is crucial to the ultimate optimization results. No software or open-source toolkit is available to estimate an SLM part's volumetric error and surface roughness. Thus, they are not considered in the validation of the estimation effectiveness. Autodesk Netfabb, a commercial software that provides the function to estimate the support volume and build time of an SLM part, can be utilized to validate the effectiveness of the proposed estimation models of support volume and build time. Table 6 presents the estimated support volumes obtained by the proposed method and Netfabb for the two MFMPs in the original orientation and OBO. The maximum error of support volume is 4.54% for the bracket. Similarly, Table 7 lists the two types of estimated build time of the two MFMPs. The maximum error is 5.02% for the bracket. The comparison results demonstrate the effectiveness of the proposed estimation methods.

To further validate the effectiveness of the proposed method for obtaining an OBO for an MFMP in SLM, the WSM commonly applied in the previous studies [13,20,34,36] is utilized to compare with the proposed method. The GA is used to solve the solution of the WSM expressed in Eq. (30). GA is a popular algorithm for solving the optimization problem, which is also provided by MATLAB software and supports vectorized calculation. Likewise, GA obtains the maximum and minimum values of the considered objectives. The weights of the considered objectives are the same as that of the proposed integrated MODM method. The population size and maximum generation are 50 and 200, respectively, and the other parameters keep the default values.

The solutions of the WSM are (0.0496°, 6.5723°) and (56.1215°, 90.0000°) for the connecting rod and bracket, respectively. The OBOs of the connecting rod and bracket obtained by the WSM and proposed methods are compared. The results are shown in Tables 8 and 9.

In Table 8, compared with the WSM, the first three objectives of the proposed method are better, especially the support volume, but the build time is worse. To quantitatively compare the effectiveness of the two methods, the proposed MODM method is applied to evaluate them in the same way as Section 4.1. The correspondence IV values are listed in Table 8, and the results suggest that the proposed method is better than the WSM.

In Table 9, compared with the WSM, although the volumetric error of the proposed method increases by 39.92%, the other three objective values are optimized;

Table 6 Comparison of support volume estimation

MFMP	Orientation	Support volume/mm^3		Difference/%
		Proposed method	Netfabb	
Connecting rod	Original	6041.10	5828.10	3.650
	OBO	2836.70	2787.60	1.760
Bracket	Original	39258.70	37961.10	3.420
	OBO	1292.50	1236.40	4.540

Table 7 Comparison of build time estimation

MFMP	Orientation	Build time/s		Difference/%
		Proposed method	Netfabb	
Connecting rod	Original	23548	24016	−1.95
	OBO	35424	35678	−0.71
Bracket	Original	50905	53597	−5.02
	OBO	45705	45809	−0.23

Table 8 Comparison of the OBOs obtained by different methods for the connecting rod

Method	$V_{\mathrm{wve}}/\mathrm{mm}^3$	$Ra_{\mathrm{wasr}}/\mu\mathrm{m}$	$V_{\mathrm{s}}/\mathrm{mm}^3$	$T_{\mathrm{b}}/\mathrm{s}$	IV
WSM	8.2895	10.7758	4654.8951	24039.8217	0.01050
Proposed method	7.8981	10.5099	2836.6676	35423.6799	0.01137

Table 9 Comparison of the OBOs obtained by different methods for the bracket

Method	$V_{\mathrm{wve}}/\mathrm{mm}^3$	$Ra_{\mathrm{wasr}}/\mu\mathrm{m}$	$V_{\mathrm{s}}/\mathrm{mm}^3$	$C_{\mathrm{build}}/\mathrm{USD}$	IV
WSM	6.6203	10.584	28077.8537	74.5537	0.00743
Proposed method	9.2628	10.573	1292.4769	64.5985	0.01470

especially, the support volume decreases by 95.40%. Similarly, the *IV* values indicate that the proposed method is better than the WSM.

The virtual manufacturing of the three orientations for the connecting rod is depicted in Fig. 12 (layer thickness is set as 1 mm for visualization), where each layer is colored with its build time. As listed in Table 8, the build time of the proposed method is higher than the WSM because the part height in the OBO obtained by the proposed method is higher than that of the WSM, which will require more recoating time. In Fig. 12, the FG's staircase effect with the highest MADR of the WSM method is more severe than the proposed method. The staircase effect of that FG of the original orientation seems to be the smallest; notwithstanding, it cannot guarantee that the last layer reaches the surface of that feature without any deviation, as shown in Table 4.

The surface roughness visualizations of the three orientations for the connecting rod are presented in Fig. 13, which verifies the results of Tables 4 and 8. The supports of the three orientations for the connecting rod are shown in Fig. 14. The OBO obtained by the proposed method has the least number of supports.

A kind of laser scanning pattern of the connecting rod in the three build orientations is depicted in Fig. 15. Each layer's cross-sectional profile changes with the change of the build orientation. This manner affects the ultimate manufacturing quality and build time and cost, among others, of the part in SLM. A desirable build orientation is crucial for practical SLM fabrication.

The virtual manufacturing with build time coloration in the three orientations for the bracket is depicted in Fig. 16. The surface roughness visualizations and supports in the three orientations for the bracket are

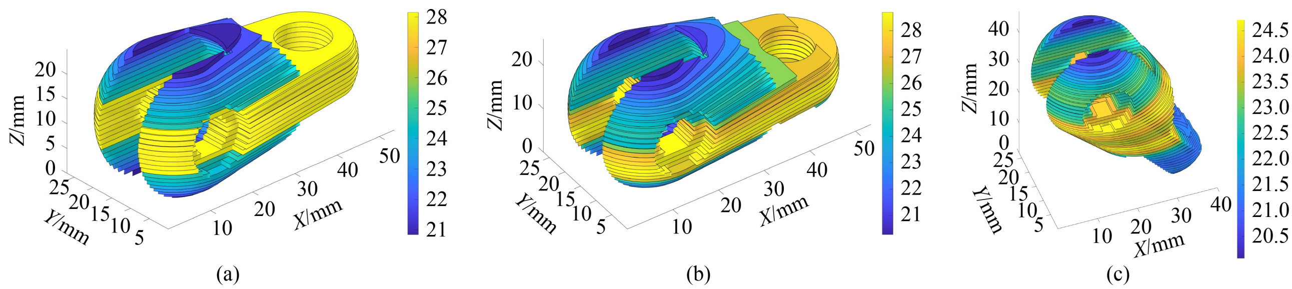

Fig. 12 Virtual manufacturing with build time coloration in different orientations for the connecting rod: (a) original orientation; optimal build orientation obtained by (b) the weighted sum model and (c) the proposed method.

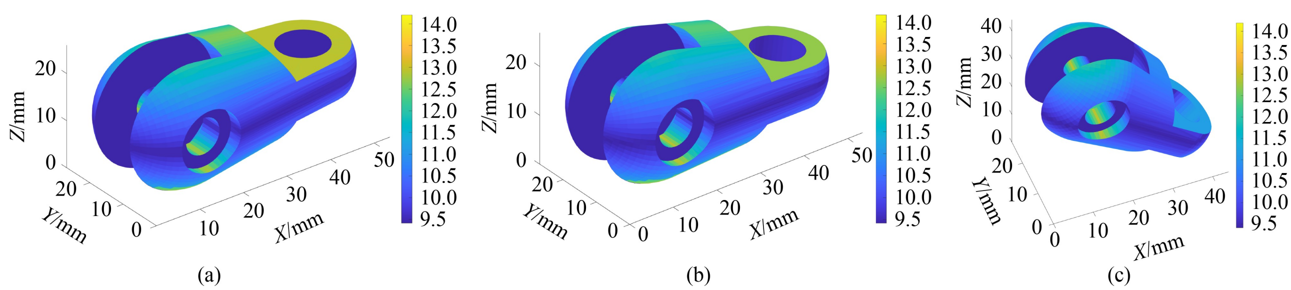

Fig. 13 Surface roughness visualizations in different orientations for the connecting rod: (a) original orientation; optimal build orientation obtained by (b) the weighted sum model and (c) the proposed method.

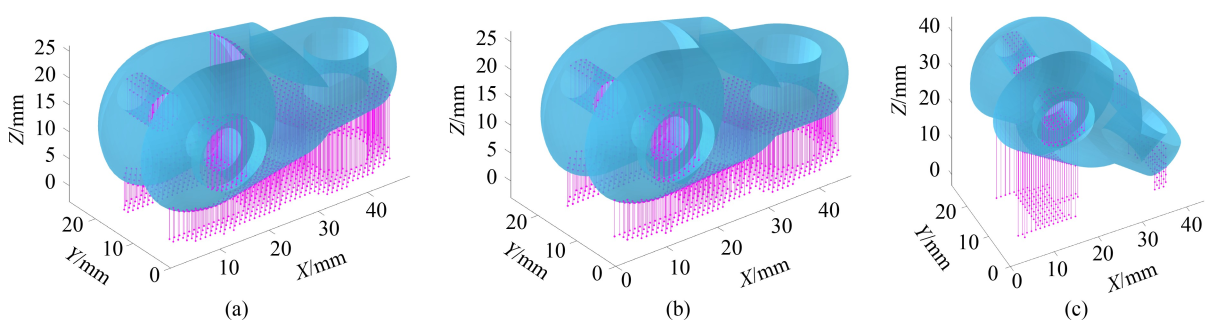

Fig. 14 Supports in different orientations for the connecting rod: (a) original orientation; optimal build orientation obtained by (b) the weighted sum model and (c) the proposed method.

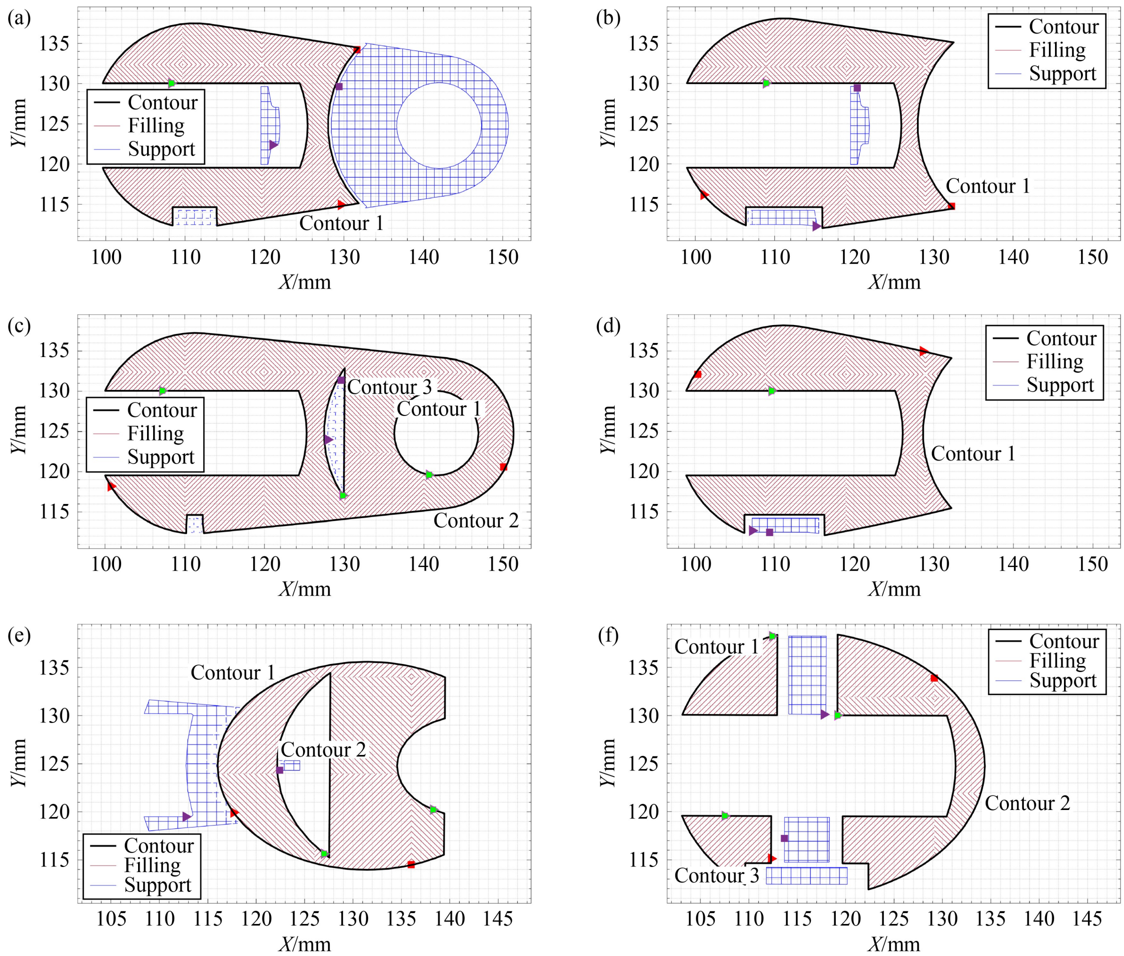

Fig. 15 Type of laser scanning pattern of the connecting rod in different part heights and orientations: (a) 35% and (b) 70% part height in original orientation; (c) 35% and (d) 70% part height in the optimal build orientation obtained by the weighted sum model; and (e) 35% and (f) 70% part height in the optimal build orientation obtained by the proposed method.

presented in Figs. 17 and 18, respectively. Similar to the connecting rod, the three figures verify the results of Tables 5 and 9. A type of laser scanning pattern for the bracket in the three orientations is illustrated in Fig. 19, which also reveals the layered cross-sectional profile's change in different build orientations.

4.3 Physical experiments

Given that the actual SLM manufacturing involves many factors, physical fabrications are conducted to validate the performance of the proposed method. The designed parts are fabricated using the ZRapid Tech iSLM280 SLM system in Ti–6Al–4V. The manufacturing volume of the machine is 280 mm (X) × 280 mm (Y) × 350 mm (Z); the laser wavelength is 1064 nm; the laser power is 500 W; the beam diameter is 0.06–0.20 mm; and the installation power is 220 V (±10%) AC 50/60 Hz, single-phase, 5/20 A.

The bracket in the three build orientations shown in Fig. 16 is fabricated, as illustrated in Fig. 20. The SLM machine and laser scanning process are presented in Figs. 20(a) and 20(b), respectively. Figure 20(c) displays the fabricated bracket in the original orientation with lattice support. Stripping the lattice support will induce extra time and cost. The SLM fabricated brackets after stripping the lattice support in the three build orientations are illustrated in Figs. 20(d)–20(f), respectively. Given the material property of Ti–6Al–4V, there exist a few support residues on the part's overhang surfaces after the support removal, as shown in the yellow squares in Figs. 20(d)–20(f). Significantly, support residues exist on the surface of the most crucial FG in the OBO obtained by the WSM, whereas the other two orientations do not exist. The support residues require further polishing.

The surface roughness measurements for the SLM fabricated brackets are performed to verify the manufacturing quality by a noncontact optical profiler, as presented in Fig. 21. The optical profiler used in the measurements is Veeco/NT9100. The objective magnification range of the optical profiler is 0.75–100 times, the vertical measurement range is 0.1–10 nm, and the resolution is 0.49 μm. The measured surface topographies of the sampling regions (Fig. 21) from the most crucial

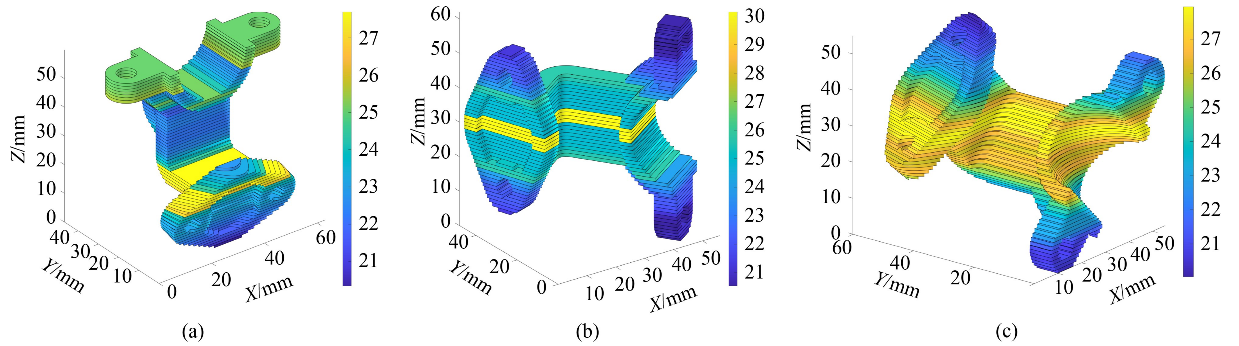

Fig. 16 Virtual manufacturing with build time coloration in different orientations for the bracket: (a) original orientation; optimal build orientation obtained by (b) the weighted sum model and (c) the proposed method.

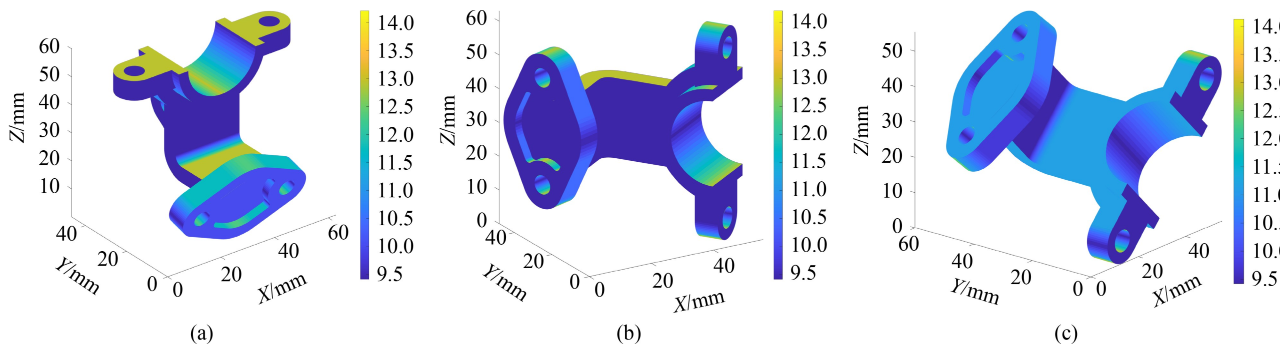

Fig. 17 Surface roughness visualizations in different orientations for the bracket: (a) original orientation; optimal build orientation obtained by (b) the weighted sum model and (c) the proposed method.

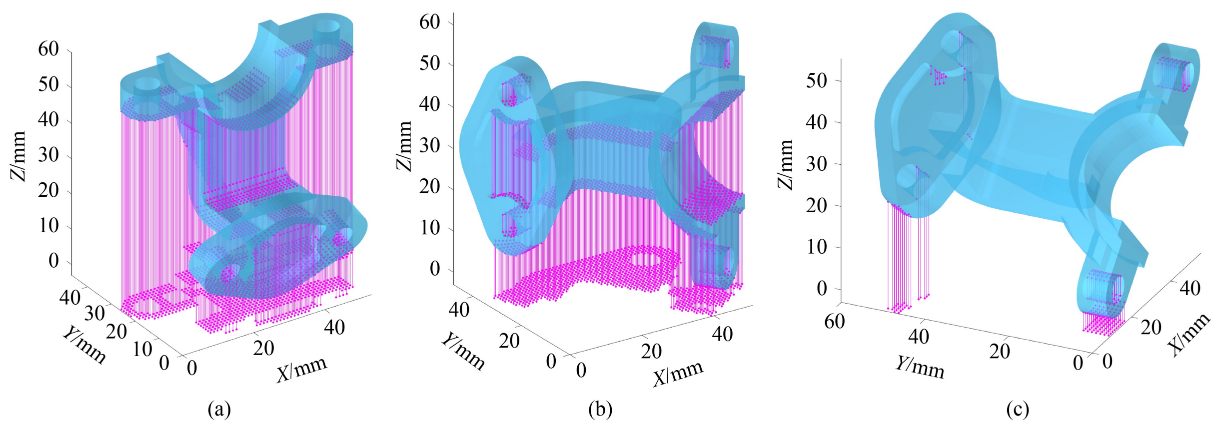

Fig. 18 Supports in different orientations for the bracket: (a) original orientation; optimal build orientation obtained by (b) the weighted sum model and (c) the proposed method.

FG for the SLM fabricated brackets are displayed in Fig. 22. For the original orientation, a slight change of the sampling region results in a noticeable difference in the surface roughness, as depicted in Figs. 22(a) and 22(b). This result implies that the sampling region's surface is uneven. This phenomenon may be because this region in the original orientation is horizontal while manufacturing. The resulting average sampling surface roughness is 15.82 μm, in which the surface roughness for Figs. 22(a) and 22(b) are 10.60 and 21.04 μm, respectively. The measured surface roughness for the OBOs obtained by the WSM and the proposed method are 10.84 and 10.62 μm, respectively. The two sampling regions in the two OBOs are vertical while manufacturing. These measurement results are similar to the previous investigations [13,57,61]. The experimental measurements demonstrate that the proposed method is desirable for better surface quality.

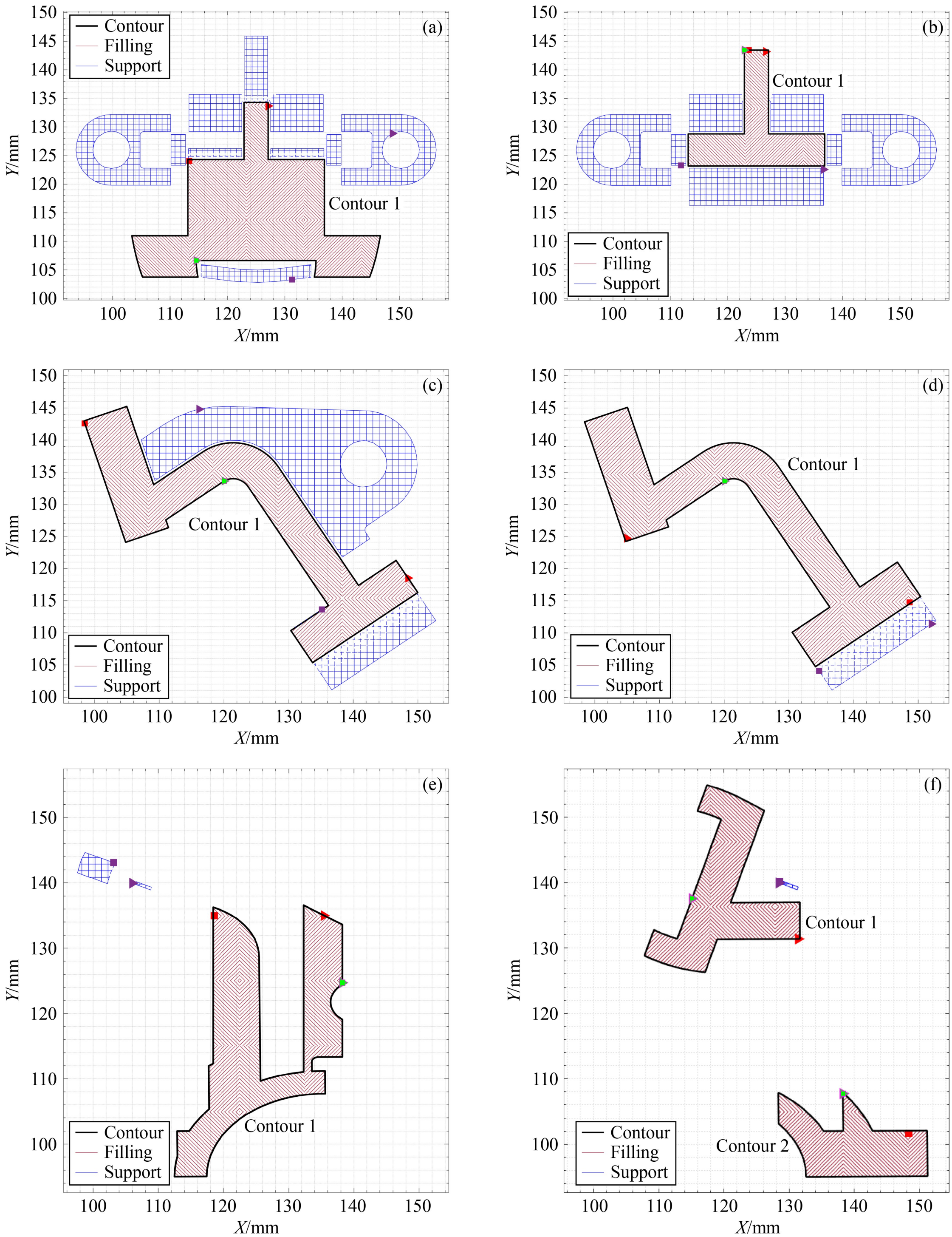

Fig. 19 Type of laser scanning pattern of the bracket in different heights and orientations: (a) 35% and (b) 70% part height in original orientation; (c) 35% and (d) 70% part height in the optimal build orientation obtained by the weighted sum model; and (e) 35% and (f) 70% part height in the optimal build orientation obtained by the proposed method.

4.4 Discussion

As shown in Figs. 9 and 10, the Pareto fronts of the connecting rod and bracket are nonconvex. As mentioned above, the WSM cannot work well in the case of MOO with nonconvex Pareto fronts [48]. The comparison results between the proposed method and the WSM in Tables 8 and 9 have verified this. Although obtaining the Pareto front will take some time, it is still worthwhile compared with the part build time, because it will bring a more accurate result that will reduce the post-processing time and cost. A more efficient solving method can be

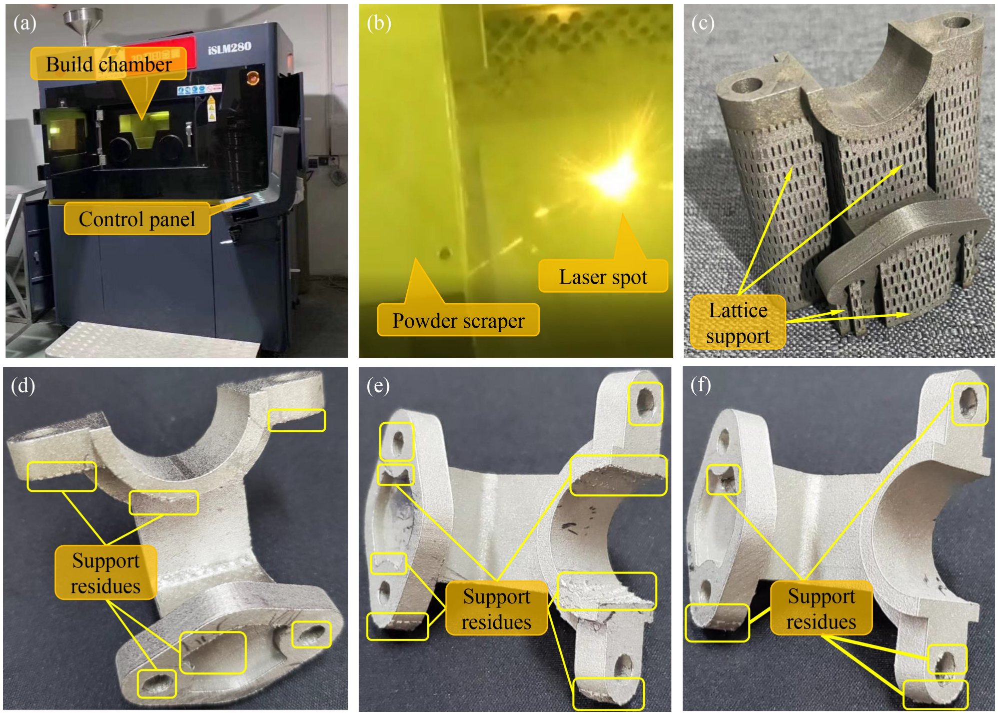

Fig. 20 Selective laser melting fabrications for the bracket in different orientations: (a) selective laser melting machine; (b) laser scanning process, (c) fabricated bracket with lattice support in original orientation; fabricated bracket after stripping lattice support in (d) original orientation, (e) the optimal build orientation obtained by the weighted sum model, and (f) the optimal build orientation obtained by the proposed method.

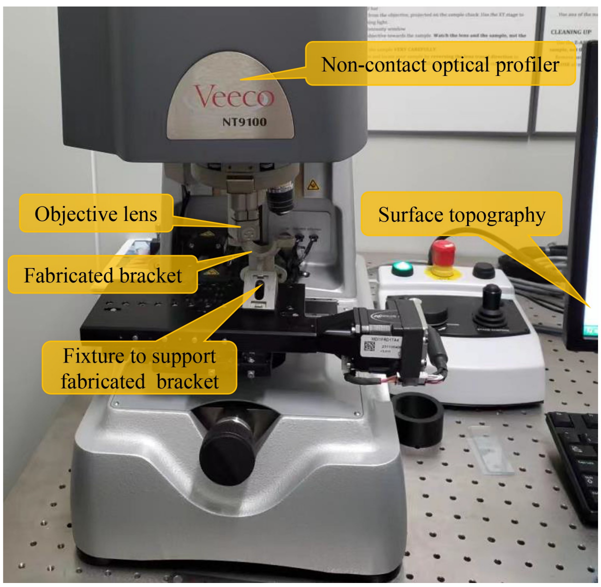

Fig. 21 Surface roughness measurement system using a noncontact optical profiler.

developed to reduce the computation cost of Pareto-based optimization (e.g., GPU acceleration computation).

This study focuses on MFMPs, and they are basically regular models. For freeform models, the surface features are difficult to identify. Indeed, if there exists a desirable feature recognition method for freeform models, the proposed method is suitable for freeform models. Without losing generality, the proposed objective estimation models are still ideal for freeform models, which requires taking the freeform model as only one FG for the volumetric error and surface roughness models. By contrast, the other three objective estimation models are naturally suitable for the freeform models.

The estimation model of the surface roughness cited from Ref. [13] is a simple reflection of the effect of build orientation, which indicates that it has accuracy and application limitations. In practice, the surface roughness of SLM parts is affected by the material properties, process parameters, and build orientation. Specific physical experiments regarding the influencing factors above are conducive to obtaining a more accurate estimation model.

The layer-by-layer melting process in SLM induces anisotropic mechanical properties for the as-built parts. Desired mechanical properties, such as tensile strength, elongation, residual stress, and Vickers hardness, are crucial for the fabrication quality of as-built parts [16]. Varying build orientations will induce different layered cross-sectional profiles (as shown in Figs. 15 and 19), which may result in various mechanical responses. Among the literature, Brika et al. [13] proposed the estimation models for the ultimate tensile strength, elongation, and Vickers for SLM parts concerning different post-processing heat treatments, using a similar

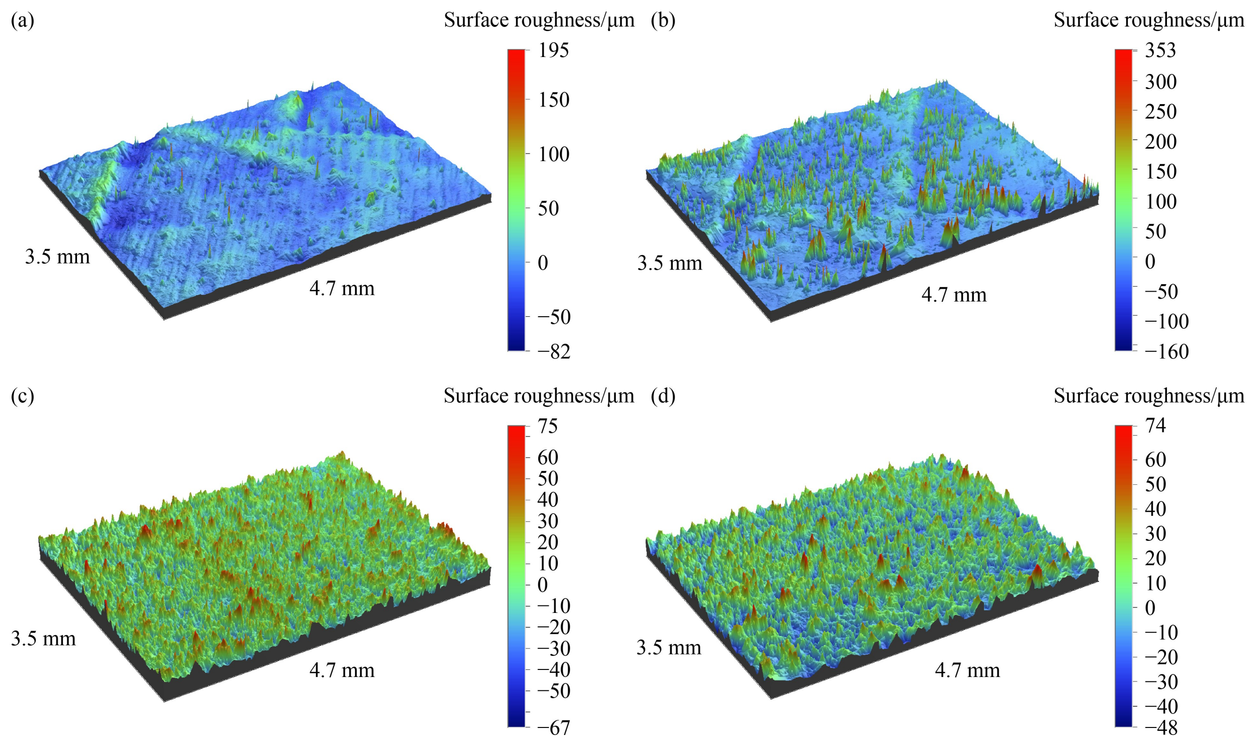

Fig. 22 Measured surface topographies of the sampling regions for the selective laser melting fabricated brackets in different orientations: (a) first and (b) second regions in original orientation; optimal build orientation obtained by (c) the weighted sum model and (d) the proposed method.

generation method to that of the surface roughness. However, the estimation models are still rough and lack adequate characterization of the synthetic effects of the process parameters and build orientation. Comprehensive and sufficient numerical and physical experiments will benefit the development of available and suitable estimation models for considering these factors in applications.

The case studies and effectiveness comparison illustrate the characteristics of the proposed method. This study focuses on determining the build orientation to benefit the manufacturing of MFMPs in SLM. To this end, an MFMP's surface features are grouped into several FGs via its MADRs, as shown in Figs. 7 and 8. The FGs are applied to the optimization objectives, namely, volumetric error and surface roughness, for mapping the MADRs of an MFMP. The estimation effectiveness comparisons of the support volume and build time models are compared with commercial software, as listed in Tables 6 and 7. The visualizations of the volumetric error, surface roughness, and support volume models are likewise presented to demonstrate the effectiveness of the estimation models, as shown in Figs. 12–14 and 16–18.

In comparison with the existing evaluation methods based on feature recognition [30–32,39,40], convex hull generation [22], facet clustering [41,42], and quaternion rotation [23,33], the proposed method obtains a more accurate result because it adopts the MOO to generate the Pareto ABOs, as shown in Figs. 9 and 10. In comparison with the WSM method [13,14,20,34,36,43,44], the proposed method obtains an OBO from the Pareto ABOs by the integrated MODM method, which is more flexible for the case of multiple conflicting objectives, as demonstrated in Tables 8 and 9.

5 Conclusions

This study proposes a method to determine an OBO for an MFMP in SLM. This method mainly consists of three steps. In the first step, the surface features of an MFMP's manifold mesh are recognized and grouped into several FGs based on their MADRs. In the second step, the estimation models of the volumetric error, surface roughness, support volume, and build time and cost are established, where the volumetric error and surface roughness values are the weighted sum of the values of the FGs. In the last step, the Pareto ABOs are obtained by the MOO regarding the considered objectives. Then, an OBO is selected from those ABOs by an integrated MODM method composed of the TOPSIS and CSM. The FAHP determines the correspondence weights for the FGs and considered objectives. Two MFMPs are tested to validate the proposed method with numerical results. The effectiveness comparisons of the estimated support volume and build time and the OBOs obtained by the WSM and the proposed method are presented. The physical fabrications and surface roughness measurements further demonstrate the performance of the proposed method. The validations indicate that the proposed method can adequately determine an OBO for an MFMP in SLM with competitive results.

As the present study concerns the build orientation of an MFMP in SLM, other crucial influencing objectives (e.g., mechanical properties) can be developed with available estimation models. In addition, more complex part geometries, such as porous shape and cellular solid, will be addressed in future work.

Nomenclature

Abbreviations

ABO	Alternative build orientation
AM	Additive manufacturing
CSM	Cosine similarity measure
FAHP	Fuzzy analytical hierarchy process
FDM	Fused deposition modeling
FG	Feature group
GA	Genetic algorithm
MADR	Machining accuracy design requirement
MFMP	Multi-feature mechanical part
MODM	Multi-objective decision making
MOO	Many-objective optimization
NSGA-II	Non-dominated sorting genetic algorithm II
OBO	Optimal build orientation
SLA	Stereolithography
SLM	Selective laser melting
SLS	Selective laser sintering
STL	Standard tessellation language
TFN	Triangular fuzzy number
TOPSIS	Technique for order of preference by similarity to ideal solution
WSM	Weighted sum model

Variables

$\widetilde{A}$	Triangular fuzzy number
A^+	Positive ideal solution
A^-	Negative ideal solution
A_g	Area of the grid generated in the projection of the bounding box on the platform
A_i^f	Area of the ith facet
A_platform	Area of the fabrication platform
B_length	Length of the part’s bounding box along the x-axis
B_width	Width of the part’s bounding box along the y-axis
C_build	Build cost of an SLM part
C_energy	Energy cost for building an SLM part
C_i	Relative closeness to the ideal solution of the ith alternative
C_i'	Normalized relative closeness to the ideal solution of the ith alternative
C_indirect	Indirect build cost of an SLM part
C_material	Material cost used for the part, support structure, and wasted material
d	Ordinate of the highest intersection point D between μ_{S_1} and μ_{S_2}
$d(S_i)$	Normalized weight of the ith object
$d'(S_i)$	Weight of the ith object obtained by the FAHP
D_i^+	Distance of the ith alternative to the positive ideal solution
D_i^-	Distance of the ith alternative to the negative ideal solution
$\boldsymbol{d}$	Build direction vector
$\boldsymbol{DM}$	Decision matrix of an MODM problem
$E_\mathrm{consumption}$	Energy consumption rate
$f_i(\theta_x, \theta_y)$	Estimation model function of the ith objective
F_i	ith facet
F_wsm	WSM evaluation value of one solution
g_i	ith object
$H_{i,j}$	Height of the jth segment of the ith supported ray
H_d^p	Hatch distance for filling the part
H_d^s	Hatch distance of the lattice support structure
H_p	Part’s height
H_pp	Height between the part and the platform
IV	Integrated MODM evaluation value
IV_i	Integrated MODM evaluation value of the ith alternative
k	Number of convex fuzzy numbers
l	Lower bound of a TFN
l_e	Edge length of the grid
$l_{g_i}^j$	Lower bound of the TFN $M_{g_i}^j$
l_t	Layer thickness
l_{S_i}	Lower bound of the TFN S_i
m	Most promising value of a TFN
$m_{g_i}^j$	Most promising value of the TFN $M_{g_i}^j$
m_{S_i}	Most promising value of the TFN S_i
M_density	Density of the material
$M_{g_i}^j$	Extent analysis value of the jth factor to the ith object
M_i	CSM value between the ith alternative and the positive ideal solution
M_i'	Normalized CSM value between the ith alternative and the positive ideal solution

M_{porosity}	Porosity of the material
$\boldsymbol{M}_{n\times q}$	Fuzzy judgment matrix used in the FAHP
n	Number of the objects
n_{f}	Number of facets of the manifold mesh model
n_{fg}	Number of the feature groups
n_{f}^{n}	Number of the facets without supports
n_{f}^{s}	Number of the facets with supports
n_{g}	Number of the grids
n_{g}^{x}	Number of the grids along the x-axis
n_{g}^{y}	Number of the grids along the y-axis
n_{o}	Number of the considered objectives
n_{r}	Number of the rays intersected with the overhang facets
$\boldsymbol{n}_i^{\text{f}}$	Unit normal vector of the ith facet
OV_i	Value of the ith objective
$OV_i^{\max}$	Maximum value of the ith objective
$OV_i^{\min}$	Minimum value of the ith objective
P_{energy}	Energy price
P_{material}	Material price
q	Number of the factors of one object
$\boldsymbol{Q}_i^{\text{fg}}$	Pairwise fuzzy comparison matrix of the feature groups of the ith part
$\boldsymbol{Q}_{\text{o}}$	Pairwise fuzzy comparison matrix of the optimization objectives
$r_{i,j}$	Normalized value of the jth objective for the ith alternative
R_{b}^{p}	Build rate of the part
R_{b}^{s}	Build rate of the support
R_{indirect}	Indirect cost rate
R_{waste}	Material waste rate
Ra_{asr}	Average surface roughness of an SLM part
$Ra_{\text{asr},i}$	Average surface roughness of the ith feature group
Ra_i^{f}	Surface roughness of the ith facet
Ra_i^{fs}	Surface roughness of the ith supported facet
Ra_{wasr}	Weighted average surface roughness of an SLM part
S_{density}	Volume fraction of the lattice support structure
S_i	Fuzzy synthetic extent concerning the ith object
T_{b}	Build time of an SLM part
T_{r}	Recoating time of each layer
u	Upper bound of a TFN
$u_{g_i}^{j}$	Upper bound of the TFN $M_{g_i}^{j}$
u_{S_i}	Upper bound of the TFN S_i
$v_{i,j}$	Weighted normalized value of the jth objective for the ith alternative
v_j^{+}	Positive ideal weighted normalized value of the jth objective among all alternatives
v_j^{-}	Negative ideal weighted normalized value of the jth objective among all alternatives
v_{s}	Laser scanning speed
V_i^{g}	Support volume of the ith grid
V_{p}	Part volume
V_{s}	Support volume of an SLM part
V_{wve}	Weighted volumetric error of an SLM part
VE	Volumetric error of an AM part
VE_i^{fg}	Volumetric error of the ith feature group
$V(S_2 \geqslant S_1)$	Degree of possibility of a TFN S_2 greater than a TFN S_1
$V(S \geqslant S_1, S_2, ..., S_k)$	Degree of possibility for a convex fuzzy number to be greater than k convex fuzzy numbers
w_i^{fg}	Weight of the ith feature group
w_i^{o}	Weight of the ith objective
$\boldsymbol{W}$	Normalized non-fuzzy weight vector
$\boldsymbol{W}_i^{\text{fg}}$	Weight vector of the feature groups of the ith part
$\boldsymbol{W}_{\text{o}}$	Weight vector of the considered objectives
x	Real value
$x_{i,j}$	Value of the jth objective for the ith ABO
α_i	Angle between the build direction and normal vector of the ith facet
θ_x	Rotation angle of the part around x-axis
θ_y	Rotation angle of the part around y-axis
ρ	Coefficient to adjust the relative importance of the TOPSIS and CSM
σ	Weight for the surface roughness calculation of a supported facet
$\mu_{\widetilde{A}}(x)$	Membership function of the TFN $\widetilde{A}$
$\mu_{S_i}(x)$	Membership function of the TFN S_i

Acknowledgements This work was funded by the National Key R&D Program of China (Grant No. 2018YFB1700700), and the National Natural Science Foundation of China (Grant Nos. 51935009 and 51821093).

References

1. Niu X D, Singh S, Garg A, Singh H, Panda B, Peng X B, Zhang Q J. Review of materials used in laser-aided additive manufacturing processes to produce metallic products. Frontiers of Mechanical Engineering, 2019, 14(3): 282–298
2. Cao Q Q, Zhang J, Chang S, Fuh J Y H, Wang H. The effect of support structures on maraging steel MS1 parts fabricated by selective laser melting at different building angles. Rapid Prototyping Journal, 2020, 26(9): 1465–1476
3. Sing S L, Yeong W Y. Laser powder bed fusion for metal additive manufacturing: perspectives on recent developments. Virtual and Physical Prototyping, 2020, 15(3): 359–370

4. Lee J M, Sing S L, Zhou M M, Yeong W Y. 3D bioprinting processes: a perspective on classification and terminology. International Journal of Bioprinting, 2018, 4(2): 151
5. Kaynak Y, Kitay O. The effect of post-processing operations on surface characteristics of 316L stainless steel produced by selective laser melting. Additive Manufacturing, 2019, 26: 84–93
6. Han W, Fang F Z. Orientation effect of electropolishing characteristics of 316L stainless steel fabricated by laser powder bed fusion. Frontiers of Mechanical Engineering, 2021, 16(3): 580–592
7. Lee J Y, Nagalingam A P, Yeo S H. A review on the state-of-the-art of surface finishing processes and related ISO/ASTM standards for metal additive manufactured components. Virtual and Physical Prototyping, 2021, 16(1): 68–96
8. Ahsan A N, Habib M A, Khoda B. Resource based process planning for additive manufacturing. Computer-Aided Design, 2015, 69: 112–125
9. Famodimu O H, Stanford M, Oduoza C F, Zhang L J. Effect of process parameters on the density and porosity of laser melted AlSi10Mg/SiC metal matrix composite. Frontiers of Mechanical Engineering, 2018, 13(4): 520–527
10. Jiang J C, Xu X, Stringer J. Optimization of process planning for reducing material waste in extrusion based additive manufacturing. Robotics and Computer-Integrated Manufacturing, 2019, 59: 317–325
11. Zhao D H, Guo W Z. Shape and performance controlled advanced design for additive manufacturing: a review of slicing and path planning. Journal of Manufacturing Science and Engineering, 2020, 142(1): 010801
12. Morgan H D, Cherry J A, Jonnalagadda S, Ewing D, Sienz J. Part orientation optimisation for the additive layer manufacture of metal components. The International Journal of Advanced Manufacturing Technology, 2016, 86(5–8): 1679–1687
13. Brika S E, Zhao Y Y F, Brochu M, Mezzetta J. Multi-objective build orientation optimization for powder bed fusion by laser. Journal of Manufacturing Science and Engineering, 2017, 139(11): 111011
14. Cheng L, To A. Part-scale build orientation optimization for minimizing residual stress and support volume for metal additive manufacturing: theory and experimental validation. Computer-Aided Design, 2019, 113: 1–23
15. Griffiths V, Scanlan J P, Eres M H, Martinez-Sykora A, Chinchapatnam P. Cost-driven build orientation and bin packing of parts in selective laser melting (SLM). European Journal of Operational Research, 2019, 273(1): 334–352
16. Kuo C N, Chua C K, Peng P C, Chen Y W, Sing S L, Huang S, Su Y L. Microstructure evolution and mechanical property response via 3d printing parameter development of Al–Sc alloy. Virtual and Physical Prototyping, 2020, 15(1): 120–129
17. Qin Y C, Qi Q F, Shi P Z, Scott P J, Jiang X Q. Status, issues, and future of computer-aided part orientation for additive manufacturing. The International Journal of Advanced Manufacturing Technology, 2021, 115(5–6): 1295–1328
18. Masood S H, Rattanawong W, Iovenitti P. A generic algorithm for a best part orientation system for complex parts in rapid prototyping. Journal of Materials Processing Technology, 2003, 139(1–3): 110–116
19. Pandey P M, Thrimurthulu K, Reddy N V. Optimal part deposition orientation in FDM by using a multicriteria genetic algorithm. International Journal of Production Research, 2004, 42(19): 4069–4089
20. Byun H S, Lee K H. Determination of the optimal part orientation in layered manufacturing using a genetic algorithm. International Journal of Production Research, 2005, 43(13): 2709–2724
21. Ahn D, Kim H, Lee S. Fabrication direction optimization to minimize post-machining in layered manufacturing. International Journal of Machine Tools and Manufacture, 2007, 47(3–4): 593–606
22. Byun H S, Lee K H. Determination of the optimal build direction for different rapid prototyping processes using multi-criterion decision making. Robotics and Computer-Integrated Manufacturing, 2006, 22(1): 69–80
23. Yu C, Qie L F, Jing S K, Yan Y. Personalized design of part orientation in additive manufacturing. Rapid Prototyping Journal, 2019, 25(10): 1647–1660
24. Di Angelo L, Di Stefano P, Dolatnezhadsomarin A, Guardiani E, Khorram E. A reliable build orientation optimization method in additive manufacturing: the application to FDM technology. The International Journal of Advanced Manufacturing Technology, 2020, 108(1–2): 263–276
25. Golmohammadi A H, Khodaygan S. A framework for multi-objective optimisation of 3D part-build orientation with a desired angular resolution in additive manufacturing processes. Virtual and Physical Prototyping, 2019, 14(1): 19–36
26. Matos M A, Rocha A M A C, Pereira A I. Improving additive manufacturing performance by build orientation optimization. The International Journal of Advanced Manufacturing Technology, 2020, 107(5–6): 1993–2005
27. Matos M A, Rocha A M A C, Costa L A. Many-objective optimization of build part orientation in additive manufacturing. The International Journal of Advanced Manufacturing Technology, 2021, 112(3–4): 747–762
28. Ulu E, Gecer Ulu N, Hsiao W, Nelaturi S. Manufacturability oriented model correction and build direction optimization for additive manufacturing. Journal of Mechanical Design, 2020, 142(6): 062001
29. Wang C F, Qian X P. Simultaneous optimization of build orientation and topology for additive manufacturing. Additive Manufacturing, 2020, 34: 101246
30. Cheng W, Fuh J Y H, Nee A Y C, Wong Y S, Loh H T, Miyazawa T. Multi-objective optimization of part-building orientation in stereolithography. Rapid Prototyping Journal, 1995, 1(4): 12–23
31. Pham D T, Dimov S S, Gault R S. Part orientation in stereolithography. The International Journal of Advanced Manufacturing Technology, 1999, 15(9): 674–682
32. West A P, Sambu S P, Rosen D W. A process planning method for improving build performance in stereolithography. Computer-Aided Design, 2001, 33(1): 65–79
33. Qie L F, Jing S K, Lian R C, Chen Y, Liu J H. Quantitative suggestions for build orientation selection. The International Journal of Advanced Manufacturing Technology, 2018, 98(5–8): 1831–1845

34. Canellidis V, Giannatsis J, Dedoussis V. Genetic-algorithm-based multi-objective optimization of the build orientation in stereolithography. The International Journal of Advanced Manufacturing Technology, 2009, 45(7–8): 714–730
35. Mele M, Campana G. Sustainability-driven multi-objective evolutionary orienting in additive manufacturing. Sustainable Production and Consumption, 2020, 23: 138–147
36. Phatak A M, Pande S S. Optimum part orientation in rapid prototyping using genetic algorithm. Journal of Manufacturing Systems, 2012, 31(4): 395–402
37. Singhal S K, Jain P K, Pandey P M, Nagpal A K. Optimum part deposition orientation for multiple objectives in SL and SLS prototyping. International Journal of Production Research, 2009, 47(22): 6375–6396
38. Padhye N, Deb K. Multi-objective optimisation and multi-criteria decision making in SLS using evolutionary approaches. Rapid Prototyping Journal, 2011, 17(6): 458–478
39. Zhang Y C, Bernard A, Gupta R K, Harik R. Feature based building orientation optimization for additive manufacturing. Rapid Prototyping Journal, 2016, 22(2): 358–376
40. Al-Ahmari A M, Abdulhameed O, Khan A A. An automatic and optimal selection of parts orientation in additive manufacturing. Rapid Prototyping Journal, 2018, 24(4): 698–708
41. Zhang Y C, Harik R, Fadel G, Bernard A. A statistical method for build orientation determination in additive manufacturing. Rapid Prototyping Journal, 2019, 25(1): 187–207
42. Qin Y C, Qi Q F, Shi P Z, Scott P J, Jiang X Q. Automatic determination of part build orientation for laser powder bed fusion. Virtual and Physical Prototyping, 2021, 16(1): 29–49
43. Paul R, Anand S. Optimization of layered manufacturing process for reducing form errors with minimal support structures. Journal of Manufacturing Systems, 2015, 36(7): 231–243
44. Chowdhury S, Mhapsekar K, Anand S. Part build orientation optimization and neural network-based geometry compensation for additive manufacturing process. Journal of Manufacturing Science and Engineering, 2018, 140(3): 031009
45. Xu J H, Sheng H S, Zhang S Y, Tan J R, Deng J L. Surface accuracy optimization of mechanical parts with multiple circular holes for additive manufacturing based on triangular fuzzy number. Frontiers of Mechanical Engineering, 2021, 16(1): 133–150
46. Mahmood M A, Visan A I, Ristoscu C, Mihailescu I N. Artificial neural network algorithms for 3D printing. Materials (Basel), 2021, 14(1): 163
47. Goh G D, Sing S L, Yeong W Y. A review on machine learning in 3D printing: applications, potential, and challenges. Artificial Intelligence Review, 2021, 54(1): 63–94
48. Zhang Q F, Li H. MOEA/D: a multiobjective evolutionary algorithm based on decomposition. IEEE Transactions on Evolutionary Computation, 2007, 11(6): 712–731
49. Chen S J, Hwang C L. Fuzzy Multiple Attribute Decision-Making Methods and Application. Berlin: Springer, 1992
50. Xia P P, Zhang L, Li F Z. Learning similarity with cosine similarity ensemble. Information Sciences, 2015, 307: 39–52
51. Nezarat H, Sereshki F, Ataei M. Ranking of geological risks in mechanized tunneling by using fuzzy analytical hierarchy process (FAHP). Tunnelling and Underground Space Technology, 2015, 50: 358–364
52. Moroni G, Syam W P, Petrò S. Functionality-based part orientation for additive manufacturing. Procedia CIRP, 2015, 36: 217–222
53. Ding D H, Pan Z X, Cuiuri D, Li H J, Larkin N, van Duin S. Automatic multi-direction slicing algorithms for wire based additive manufacturing. Robotics and Computer-Integrated Manufacturing, 2016, 37: 139–150
54. Xu J H, Sheng H S, Zhan J T, Zhang S Y, Tan J R. Assembly-free design for additive manufacturing of articulated components based on layered precision assignment. International Journal of Computer Integrated Manufacturing, 2022, 35(9): 909–926
55. Strano G, Hao L, Everson R M, Evans K E. Surface roughness analysis, modelling and prediction in selective laser melting. Journal of Materials Processing Technology, 2013, 213(4): 589–597
56. Triantaphyllou A, Giusca C L, Macaulay G D, Roerig F, Hoebel M, Leach R K, Tomita B, Milne K A. Surface texture measurement for additive manufacturing. Surface Topography: Metrology and Properties, 2015, 3(2): 024002
57. Tian Y, Tomus D, Rometsch P, Wu X H. Influences of processing parameters on surface roughness of HastelloyX produced by selective laser melting. Additive Manufacturing, 2017, 13: 103–112
58. Yan X C, Gao S H, Chang C, Huang J, Khanlari K, Dong D D, Ma W Y, Fenineche N, Liao H L, Liu M. Effect of building directions on the surface roughness, microstructure, and tribological properties of selective laser melted Inconel 625. Journal of Materials Processing Technology, 2021, 288: 116878
59. Alghamdi A, Downing D, McMillan M, Brandt M, Qian M, Leary M. Experimental and numerical assessment of surface roughness for Ti6Al4V lattice elements in selective laser melting. The International Journal of Advanced Manufacturing Technology, 2019, 105(1–4): 1275–1293
60. Balbaa M, Mekhiel S, Elbestawi M, McIsaac J. On selective laser melting of Inconel 718: densification, surface roughness, and residual stresses. Materials & Design, 2020, 193: 108818
61. Feng S C, Kamat A M, Sabooni S, Pei Y T. Experimental and numerical investigation of the origin of surface roughness in laser powder bed fused overhang regions. Virtual and Physical Prototyping, 2021, 16(sup1): S66–S84
62. Möller T, Trumbore B. Fast, minimum storage ray-triangle intersection. Journal of Graphics Tools, 1997, 2(1): 21–28
63. Calignano F. Design optimization of supports for overhanging structures in aluminum and titanium alloys by selective laser melting. Materials & Design, 2014, 64: 203–213
64. Liu J K, Chen Q, Liang X, To A C. Manufacturing cost constrained topology optimization for additive manufacturing. Frontiers of Mechanical Engineering, 2019, 14(2): 213–221